BNL-69633

AIRBORNE MEASUREMENT OF INORGANIC IONIC COMPONENTS OF FINE AEROSOL PARTICLES USING THE PILS-IC TECHNIQUE DURING ACE-ASIA AND TRACE-P

Y.-N. Lee
Atmospheric Sciences Division, Brookhaven National Laboratory, Upton, NY 11973

R. Weber, Y. Ma, D. Orsini, and K. Maxwell
School of Earth and Atmospheric Sciences, Georgia Institute of Technology, Atlanta, GA 30332

D. Blake and S. Meinardi
University of California, Irvine, CA 92697

G. Sachse and C. Harward
NASA Langley Research Center, Hampton, VA 23681

T. Anderson and S. Masonis
Department of Atmospheric Science, University of Washington, Seattle, WA 98195

A. D. Clarke, K. Moore, and V. N. Kapustin
School of Ocean and Earth Science and Technology, University of Hawaii, Honolulu, HI 96822

T.-Y. Chen
Institute of Geophysics, Academia Sinica, Taipei, Taiwan

D. C. Thornton, F. H. Tu, and A. R. Bandy
Department of Chemistry, Drexel University, Philadelphia, PA 19104

November 2002

Prepared for
Journal of Geophysical Research

By acceptance of this article, the publisher and/or recipient acknowledges the U.S. Government's right to retain a nonexclusive, royalty-free license in and to any copyright covering this paper.

Research by BNL investigators was performed under the auspices of the U.S. Department of Energy under Contract No. DE-AC02-98CH10886.

Abstract

Fine aerosol particle ($D_p < 1$ μm) contents of NH_4^+, SO_4^{2-}, NO_3^-, Ca^{2+}, K^+, Mg^{2+}, Na^+, and Cl^- were determined at a 4-min time resolution using a particle-into-liquid-sampler coupled to ion chromatography analysis (PILS-IC) on board the NCAR C130 and NASA P-3B aircraft during the 2001 Aerosol Characterization Experiment (ACE)-Asia and Transport and Chemical Evolution over the Pacific (TRACE-P), respectively. The maximum total ion mass concentrations observed during ACE-Asia and TRACE-P were 27 μg m^{-3} and 84 μg m^{-3}, respectively. During ACE-Asia, NH_4^+ and SO_4^{2-} dominated with the dust derived Ca^{2+} contributing nearly equally as SO_4^{2-} in mixing ratios. Sea-salt derived Na^+ and Cl^- were comparable to biomass burning tracer K^+, all showing > 1 ppbv only in the top one percent population. During TRACE-P, NH_4^+ dominated, followed by SO_4^{2-}, Cl^-, Na^+, NO_3^-, Ca^{2+} and K^+, in decreasing order of importance. Mg^{2+} was derived mainly from dust and was small, but was large when sea-salt particles were important. In both campaigns, NH_4^+, SO_4^{2-}, NO_3^-, CO and black carbon were strongly correlated, indicating that combustion was the dominant source of these species and that NH_3 was in sufficient supply as a neutralizing agent. The molar ratios of $[NH_4^+]$ to $[NO_3^-] + 2[SO_4^{2-}]$ were identical in the two campaigns, ~0.70, with important deviations observed only in volcano plumes whereby elevated aerosol sulfate was found to correlate with SO_2. Charge balance of the measured ions showed both positive and negative deviations from neutrality; the magnitudes of which (~20 % at total ion ≥ 3 ppbv, independent of altitude) provide estimates of the unmeasured anions (e.g., carboxylates) and cations (e.g., H^+, Fe, amines). Significant mixing of pollution derived NO_3^- and SO_4^{2-} and dust derived Ca^{2+} frequently occurred, making it difficult to assess the contribution of mineral particle surface mediated NO_3^- production.

1. Introduction

Atmospheric aerosol particles play many important roles in the environment, including visibility, Earth radiation budget and human health effects (NRC, 1998). In order to establish an ability to predict the distribution of aerosol particles (in terms of size, number and mass loading) and to assess their environmental and health effects, characteristics of various types of aerosol sources from different regions of the world are a prerequisite knowledge needed as input to model calculations. Since many Asian countries are experiencing increased energy consumption accompanying rapid economical growth, the associated emissions related to man-made activities are expected to rise significantly. This increased emission can impact chemical composition of the atmosphere on a regional to global scale and must be carefully monitored to evaluate their current effects and to predict their future changes. In addition to emission sources related to man-made activities, natural sources of aerosol particles and their precursors also need to be understood. In Asia, both biomass burning and dust storms are important processes by which aerosol particles are generated.

To gain an understanding of the various emission sources, two major field measurement programs were carried out to record the chemical signals of outflows from Eastern and Southeastern Asia. Transport and Chemical Evolution over the Pacific (TRACE-P) was an aircraft-based campaign organized by US National Aeronautics and Space Administration (NASA). This program used two large research aircraft, a DC-8 and a P-3B, to measure chemical composition mainly off the coast of China, Taiwan, Japan and Korea during the period between March 4 and April 4, 2001. Aerosol Characterization Experiment (ACE)-Asia was organized by National Science Foundation (NSF) and National Oceanographic and Atmospheric Administration (NOAA) involving ground (in Taiwan, China and Korea), shipboard (NOAA

R/V Ron Brown), and aircraft (NSF C-130) measurements. The NSF C-130 flew mainly over the waters off the coast of China, Japan and Korea during the period between March 30 and May 3, 2001.

Participating in both of these programs, we made real-time determination of concentrations of inorganic ionic components in fine aerosol particles (i.e., aerodynamic size diameter <1 μm) on board the NASA P-3B and the NSF C-130 aircraft using a recently developed technique, particle-into-liquid-sampler coupled to ion chromatography analysis (PILS-IC) (Weber et al., 2001; Lee et al., 2002; Orsini et al., 2002). Eight species, NH_4^+, SO_4^{2-}, NO_3^-, Ca^{2+}, K^+, Mg^{2+}, Na^+, and Cl^- were determined at a time resolution of 4 min and a limit of detection (LOD) of ~0.05 μg m^{-3}. We present in this paper a brief description of the principles and operation of the PILS-IC instrument, an overview of the data collected on the two aircraft platforms, and an analysis of the relationships and possible sources of these chemical components in conjunction with other simultaneously measured data.

2. Experimental Section

PILS-IC Instrument. The PILS-IC instruments used on the two aircraft were identical and consisted of three major components: a condensational particle growth chamber, an impactor sample collector, and an IC analysis system (Figure 1). Sample air drawn into the PILS (15.0 L min^{-1}) was mixed with steam (from 1.0 mL H_2O, at 110 °C) to create a supersaturation condition under which aerosol particles were grown to supermicron sizes. The resulting large droplets were collected using an impactor designed with a D_{50} = 1 μm (Marple and Willeke, 1976). The small liquid sample collected on the impactor surface was washed with a constant stream of H_2O at a flow rate of 0.20 mL min^{-1} and carried to the IC systems. We refer to this flow as the carrier flow. The computer controlled IC analysis system consisted of one IC unit for the anions

(Metrohm model 761 with a suppressor, equipped with a Metrohm Supp-5, 4 x 100 mm, anion column) and one IC unit for the cations (Metrohm model 761 without a suppressor, equipped with a Metrohm Metrosep Cation 1-2, 4 x 125 mm, column). The eluants were 4.0 mM Na_2CO_3/2.0 mM $NaHCO_3$ in H_2O and 4.0 mM tartaric acid in 10% CH_3CN/H_2O for the anion IC and cation IC, respectively. Eluant flow rates were both maintained at 1.0 mL min^{-1}. Since the actual sample volume (from the collected droplets) varied depending on number concentration of the condensable particles, the degree of dilution resulting from mixing the sample with the constant carrier flow also varied albeit in a narrow range. To determine this dilution factor, $LiClO_4$ at 2.0 μM in H_2O was used as the carrier flow. The dilution factor was then determined from the concentration of Li^+ also determined by the cation IC. Potential gaseous interferents, e.g., NH_3, HNO_3, were removed using two honeycomb denuders in series upstream of the PILS coated with citric acid and Na_2CO_3 for alkaline and acidic gases, respectively (Sioutas et al., 1996).

Inlet Systems. The aerosol inlets to the PILS-IC systems on the NSF C130 and the NASA P-3B were different: the C-130 featured a Low Turbulence Inlet (LTI) which allowed high transmission efficiencies for large size aerosol particles (upward of 40 μm) and the P-3B used a shrouded inlet which maintained an attack-angle independent turbulence characteristics in the diffuser cone. Despite of these differences, since the sample air-steam mixing region of the PILS was found to effect a 50% cut-off size of 1.3 μm at the 15.0 L min^{-1} sample flow rate used (Orsini et al., 2002), the two aircraft inlets were considered nearly identical concerning the transmission efficiencies of the upper end of particle size range important to the PILS. However, because a much longer connection was required on the P-3B between the aerosol inlet and the

PILS, there remained a possibility that the P-3B PILS experienced a slightly lower efficiency for larger size particles due to line losses.

Collection Efficiency. The instrument's sampling efficiency for smaller particles levels off at about 87% (Orsini et al., 2002). This agreed with filter data collected during TRACE-P to monitor the performance of the instrument. We recommend multiplying the reported data in the data archive by a factor of 1.15 to correct for this efficiency.

Other measurements. Hydrocarbons were determined by taking whole air samples in electro-polished canisters followed by laboratory GC-FID-MS analysis (Blake et al, 1997). CO was measured by a tunable diode laser absorption spectroscopy technique (Sachse et al., 1991) and SO_2 was by a chemical ionization mass spectrometry technique (Thornton et al., 2002). The techniques used to determine aerosol optical properties including scattering and absorption as a function of wavelength and particle size are reported in companion papers in this special issue (e.g., Anderson et al. 2002; Howell et al., 2002).

Flight summary. A total of 19 research flights were performed on each aircraft. All of the 19 flights of the NSF C-130, which was stationed in Iwakuni, Japan, were made over Japan, South Korea, the Yellow Sea, East China Sea, and the Sea of Japan (between Lat 23-43 deg N and Lon 124-144 deg E , Fig. 2). In contrast, the NASA P-3B devoted a total of 7 research flights over the Pacific Ocean during the ferry trips between California and Asia, leaving 12 flights covering the western Pacific region including South China Sea and the region mentioned above. We limit our analysis to TRACE-P data that were collected in this area, i.e., Lat 7-41 deg N and Lon 112-156 deg E (Figure 2). During this research phase, the P-3B was stationed in Hong Kong, Okinawa, and Yokota, Japan. The two aircraft missions overlapped for 5 days during which two intercomparison flights were attempted on 3/30/01 and 4/1/01. Concerning the PILS

measurement, no data were obtained on the C130 on 4/1/01 because of an instrument problem. Intercomparison of the PILS-IC data collected on the two aircraft on 3/30/01 is to be reported by Ma et al. (2002a). The ceilings of the two aircraft were comparable: 7 km and 8 km for the P-3B and the C130, respectively. The durations were 8-10 hr.

3. Results and Discussion

PILS-IC data were collected on all of the 19 research flights on the NASA P-3B. On the C-130 the data are missing on 3 flights: RF02 (4/1/01), RF03 (4/4/01) and RF19 (5/3/01). The vertical distributions of the ions and the total ion mass concentration in three latitude bands are shown in Figure 3 and Figure 4, respectively. Noting that NH_4^+, NO_3^-, and SO_4^{2-} all showed much lower concentrations above 3 km, we used this altitude as an approximate division between the mixed layer and the free troposphere for displaying the probability plots of the ions (Figure 5). The maximum total ion concentration observed on the P-3B was significantly higher (84 μg m^{-3}) than that of the C130 (27 μg m^{-3}) mainly because of an encounter of a highly polluted air mass in the Yellow Sea. Concentrations of Na^+ and Cl^- were both higher on the P-3B, but K^+ concentration were roughly comparable. The C130 however intercepted air masses that contained much higher Ca^{2+} than the P-3B, maximum being 6 ppbv vs 2.5 ppbv.

<u>Relationships between the ions</u>. Individual chemical components are useful tracers for identifying their sources (e.g., Andreae and Merlet, 2001). The relationship between these species, whether with a strong correlation or the lack of it thereof, provides additional support for such analyses. Na^+ and Cl^- are thought to be primarily derived from sea-salt aerosols especially in marine environment where the ACE-Asia and TRACE-P experiments were conducted. During ACE-Asia the plot of Cl^- against Na^+ showed a slope of 1.04 with $r^2 = 0.84$ (C130, Figure 6), fairly close to the seawater ratio of 1.16. Several data points showing high Na^+ but very low

Cl^- were not used in the regression for possible overestimation of the Na^+ concentrations. The slightly lower ratio observed is consistent with acidification of the particles which results in a Cl^- deficit through HCl volatilization. The correlation between Cl^- and Na^+ observed during TRACE-P showed a higher slope of 1.4 (Fig. 6), suggesting possible additional source of Cl^- other than sea-salt aerosols. Since the three highest Cl^- points were found at an altitude of 3-4 km and were associated with moderate Ca^{2+} concentrations, ~500 pptv, a source of Cl^- in crustal material cannot be ruled out. Alternatively, we cannot rule out the possibility that these high concentrations of Cl^- were overestimated.

In the C130 data set, Mg^{2+} showed a correlation with Ca^{2+} ($r^2 = 0.83$) with a slope of 0.12, but not with Na^+ (Figure 7). However, in the P-3B data set, we noted that Mg^{2+} at elevated concentrations (>400 pptv) were correlated with Na^+ ($r^2 = 0.78$) having a Mg^{2+} to Na^+ ratio of 0.08. This slope is fairly close to the seawater ratio of 0.11. When these high Mg^{2+} points are removed, Mg^{2+} showed a correlation with Ca^{2+} ($r^2 = 0.69$) and a Mg^{2+} to Ca^{2+} ratio of 0.16, similar to that found on the C130. These results are consistent with the general conditions the two aircraft platforms had experienced: the C130 saw more dust than sea-salt and the P-3B the opposite.

K^+ showed a moderate correlation with NH_4^+ ($r^2 = 0.47$) and NO_3^- ($r^2 = 0.64$). Because K^+ is thought to be associated with biomass (including biofuel) burning, these correlations suggest that both NH_4^+ and NO_3^- have an appreciable source in these processes. A detailed analysis of K^+ as a biomass burning tracer is reported by Ma et al (2002a) based on TRACE-P data.

NH_4^+ strongly correlated with NO_3^- ($r^2 = 0.73$) and SO_4^{2-} ($r^2 = 0.88$), and stronger still with the sum of NO_3^- and SO_4^{2-} (Figure 8), suggesting that NH_3 shared common emission

sources with NO_3^- and SO_4^{2-} and their precursors. If a slope of unity was observed, then it would mean a complete neutralization of HNO_3 and H_2SO_4 by NH_3. However, since the best fit slope was 0.68, it indicates that on average there is a ~30% of deficit in NH_4^+ compared to NO_3^- and SO_4^{2-}. This deficit is therefore made up by other cations, including possibly the hydronium ion (acid aerosols), organic species (e.g., amines), and soil derived species (e.g., Ca, Fe and Mn). The altitude dependence of the ratio of NH_4^+ to the sum of NO_3^- and SO_4^{2-} is shown in Figure 9. The locally weighted regression scatterplot smoothing (Lowess) shown as the solid line, which approximates the median, indicates for the C130 data a slight negative departure from the best fit slope of 0.68 in the 3 to 6 km range and a positive departure above 6 km. For the P-3B data, the ratio decreased from ~1 at low altitude to ~0.5 at high altitude. We used the Lowess fit because it was more convenient than the approach of showing box plots of binned data (in this case, binned according to altitude).

Co-emission of alkaline NH_3 along with aerosol sulfate and its precursor SO_2 is also observed during a study of the plume of the Miyakejima volcano (24.08N, 139.53E, P-3B flight no.17, 3/27/2001). Sampling was carried out approximately 200 to 300 km downwind of the volcano to the east southeast of the volcano. The molar ratio of $[NH_4^+]$ to $2[SO_4^{2-}]$ decreased with increasing aerosol SO_4^{2-}, reaching an asymptotic value of 0.42 ± 0.016 (Fig. 10). Because the analysis was confined to data points that were associated with the volcanic plume (altitude < 2km; $[SO_2] > 2$ ppbv), the reaching of a NH_3 to SO_4^{2-} equivalent ratio at 0.42 indicates that NH_3 was released at a molar ratio similar to or greater than that of SO_2. It is noted that SO_4^{2-} was correlated with SO_2 (Figure 11) suggesting that the oxidation of SO_2 to H_2SO_4 is the rate limiting step of SO_4^{2-} production. Because we expect a titration behavior to be observed in the $[NH_4^+]/[SO_4^{2-}]$ ratio if NH_3 is the only neutralizing reagent, the fact that the ratio leveled off at

0.42 without showing an end point strongly suggests the presence of other alkaline materials. We speculate that amines were among the candidates.

Charge Balance. Charge balance of the observed aerosol ionic components offers insights into whether the major ionic species comprising the aerosol particles have been identified and quantified and, in case of departure from neutrality, the possible identities of the missing ionic species and the magnitude of their contributions. In addition, measurement reliability can also be gauged through this examination.

In Figure 12 we plot the total positive charges against the total negative charges (in pptv-equivalent) found in the samples. For the C130 data set, the best fit shows a slope of 0.91 and a large intercept of 648 pptv-eq. The correlation coefficient of this scatter plot is 0.67, reflecting the fairly sizable scatter of the data. However, we noted that all the points lie above the 1:1 ratio line contained elevated levels of Ca^{2+}, i.e., $[Ca^{2+}] > 1.0$ μg m^{-3}. A plausible explanation of this observation is that the anions associated with Ca^{2+} were not completely identified by our measurement technique. A possible candidate of this missing anion is CO_3^-, which is known to be associated with crustal material derived Ca^{2+} and was not quantified by our IC technique.

To examine whether all of the anions associated with Ca^{2+} were undetected and therefore resulted in the large positive deviations seen in Figure 12, we plot the same data but with Ca^{2+} removed from the total positive charge (Fig. 12). While the correlation coefficient increased to 0.80, the best fit slop only slightly lowered to 0.82, with large scatters evenly distributed about the 1:1 line. This indicates that Ca^{2+} rich samples with potentially unquantified anions contributed only a portion of the positive deviation in the charge balance. It was noted that neither Cl^- nor SO_2 caused a bias in the observed scatter; data points with high values of these two species were roughly evenly distributed about the 1:1 ratio line. With the aerosol chemical

composition knowledge already established (e.g., Seinfeld and Pandis, 1997), we recognize that organic matters are also important components of aerosols. It is conceivable that organic acids (carboxylic acids) and bases (amines) were at least partially responsible for the charge balance deviations observed here (e.g., Rogge et al., 1993; Kawamura, 1999). Negative deviation in the charge balance, i.e., deficit in positive charges, may also reflect the presence of strong acid, principally sulfuric acid, whereby the hydronium ion was not determined. The red data points (Fig. 12) exhibiting the largest negative deviations are those identified in Figure 8 having the lowest ratio of NH_4^+ to (NO_3^-+SO_4^{2-}), suggesting that the strong acid, H_2SO_4, might not be fully neutralized and were responsible for the observed negative deviation.

The plots of total positive to negative charges are given in Figure 13 for the P-3B data. As with the C130 data, samples contained higher Ca^{2+} tended to lie above the 1:1 line. The best fit slope, 0.83, is similar to that of the C130 data with Ca^{2+} removed. However, we noted that samples corresponding to high SO_2 concentration were responsible for a lower positive to negative charge ratio. The red points in Figure 13 with SO_2 in excess of 10 ppbv were identified to be those collected in the Miyakejima volcano plumes during P-3B flight 17. It is interesting to see that some of the high SO_2 points which were not associated with the volcanic plumes showed a charge balance very close to unity, again supporting the notion that alkaline material, principally NH_3, is co-emitted at a level similar to the acid aerosols and their precursors. There are fewer data points in this figure because SO_2 was not determined on all the P-3B flights.

The magnitude of the charge imbalance, i.e., total positive charges minus total negative charges, is plotted in Figure 14 as a function of the total concentration of the ions. Since we did not include Ca^{2+} in this plot, the magnitude of positive deviations indicated in Fig.14 represent a minimum as some of the anions associated with Ca^{2+} such as SO_4^{2-} which are not removed along

with Ca^{2+} would give rise to a negative bias to this ion imbalance. The Lowess fit of the negative deviations showed a "median" of -60% at the lowest total concentration which then decreased to -18 % at 3 ppbv and remained at that level for the higher concentration regime. The Lowess fit of the positive deviations reduced from 37% at the lowest concentration to 24% at 3 ppbv, and then remained between 20 to 15% for the higher concentration range. The P-3B data showed a similar magnitude of percent deviation from neutrality but slightly more negative within the concentration range of the C130 (maximum 14 ppbv).

Since the limit of detection of the PILS-IC were 10 ng m^{-3} and 50 ng m^{-3} for the anions and cations, respectively (Orsini et al., 2002), we estimated a measurement uncertainty in the total anion to be ~10 pptv and total cations to be ~110 pptv. The total uncertainty in the ion imbalance calculation is ~110 pptv, being dominated by the cations' uncertainty. It is clear that this small measurement uncertainty contributed negligibly to the observed scatter in Fig. 14, accounting for only 10% at a total concentration as low as 1 ppb. One notes that the higher LOD for cations may be responsible for a larger negative deviation at the lowest aerosol mass loading.

It should be pointed out that one should not consider only those samples exhibiting charge imbalance to have unidentified organic ions. Since neither organic cations and anions nor the strong acid, hydronium, were detected, it is unlikely that we can rule out these components for samples that did show a reasonable charge balance. Two corollaries that follow are: (1) no a priori expectation of a normally distributed charge balance centered at zero, and (2) the missing charges cannot be used as a surrogate for the concentrations of missing organic ionic species.

<u>Altitude dependence of charge imbalance</u>. We plot the charge imbalance (with and without Ca^{2+}) as a function of altitude in Figure 15 to inspect whether the imbalance exhibits any altitude dependence. The Lowess fits of the C130 data show that the surrogate median value is

very near zero at the lowest altitude, and increases with increasing altitude reaching ~60% at the maximum altitude of 8 km. With Ca^{2+} ion removed from the charge imbalance calculation, the median remains at ~zero from the lowest altitude to 5 km and then increases to ~30% at the highest altitude. The data points with total ion concentration less than 500 pptv which should show the largest percent measurement uncertainties (≥ 20%, solid circles, Fig.15) did not show a significantly different pattern in either magnitude or sign of the departure from the remaining data, indicating that measurement uncertainties contributed insignificantly to the observed charge imbalance. On the other hand, the P-3B data which included Ca^{2+} showed an increase in positive deviation with increasing altitude, similar to the C130 data. The lower concentration data points (total ion < 500 pptv, solid circles) appeared to exhibit a wider spread in the imbalance, suggesting that the measurement uncertainty may have played a role in this quantity.

Relationships of aerosol ionic components with other chemical and physical measurements. Submicron aerosol particles are known to have an important source in combustion processes which produce precursors such as SO_2, hydrocarbons, and NO_2 in addition to primary particulate matter such as soot containing particles. Since CO is a major byproduct of combustion, a correlation between CO and fine aerosol mass loading (and some aerosol chemical components) is expected. In Figure 16 we plot the sum of the concentrations of NH_4^+, SO_4^{2-}, NO_3^-, and K^+ against CO. Na^+, Cl^-, Ca^{2+}, and Mg^{2+} were not included because they are considered non-combustion related. Although the majority of the ACE-Asia data points conform to a fairly strong correlation (Fig. 16), there is a separate group of data that showed much smaller ratios. Since these data points also correspond to similarly low ratios of other species to CO, e.g., toluene and ethane, we surmise that these data points were collected in air masses that had been substantially processed leaving the long lived CO relatively unchanged.

To investigate this possibility, we establish a time scale that can approximate the photochemical age of an air mass. Ratios of co-emitted hydrocarbons, e.g., benzene and toluene from automobile exhausts, have been applied to determining the plume age (Gelencser et al., 1997). While this approach has the advantage of being insensitive to dilution, good knowledge of the ratio of the hydrocarbons at the source is required. Further, a realistic average OH concentration is also needed. Since fairly large uncertainties exist in both quantities, the photochemical age estimated can only be qualitative. However, somewhat favorable for the ACE-Asia and TRACE-P environment is that there are fewer nearby sources over the ocean that can affect this ratio.

From a selected hydrocarbon species available we used ethyne and toluene for this calculation because both are known to have a strong source in vehicular emissions. Using a source ethyne/toluene ratio of 0.65 (Fraser et al., 1998) and a 24-hr average [OH] of 5.5×10^6 cm^{-3}, we derived a photochemical age of 8 hr to 51 hr. This time scale was found to agree with the one established using propane and toluene to within 10 hrs. Although the group of data in Fig. 16 showing a small ion mass to CO ratio were somewhat aged, 30 to 51 hr, there are significantly more data points in this age group belonged to the higher slope group of Fig. 16. Consequently, it is clear that photochemical reactions (within ~2 days) were not the primary process by which aerosols were removed from the atmosphere. Cloud processing which preferentially removes soluble species must be responsible for these data points.

It should be pointed out that there is a possibility that some points in this high CO-low aerosol mass group may have been overestimated because many points in this group corresponded to a near zero CN concentration. In either case, we have treated the two groups separately with their own best fits. We noted that the inclusion of the non-combustion related

ions mentioned above did not affect the correlation, r^2 remaining at 0.82. This is not unexpected concerning Na^+ and Cl^- as their concentrations were low. However, this also indicates that Ca^{2+} which was present at much higher concentrations had been relatively well mixed with combustion plumes. Furthermore, it's worthwhile noting in Fig. 16 that samples containing elevated K^+ are associated with the highest CO. Since K^+ is believed to be a tracer for biomass (and biofuel) burning, the inefficient combustion process which is known to generate a significant amount of CO is corroborated by this observation.

A similar analysis is made for the TRACE-P data in Figure 16. Although K^+ is again found to be associated with high CO concentrations, the data did not form clearly distinguishable groups like the ACE-Asia data. We nonetheless fitted the data without the group which showed [Ion] less than 2 ppbv and [CO] greater than 300 ppbv. These samples were found to have elevated CH_3Cl (600-1000 pptv), but contained essentially zero K^+, consistent with cloud processing which had preferentially removed the soluble species. The altitude at which these points were sampled ranged between 0.6 and 6 km with 2/3 of them above 2 km. The eyeballed maximum slopes using the top of the data envelops are not too different between the two data sets, providing a qualitative estimate of the maximum ion concentration can be expected from the CO emitted, ~5%.

<u>Relationship between Ca^{2+} and NO_3^-.</u> Ca^{2+} (and other mineral cations) contained in dust aerosols serves as an important neutralizing and quenching reagent for acids produced in the gas phase (e.g., nitric and sulfuric acids). Although it has been suggested that mineral particle can also mediate chemical transformation (Dentener et al., 1996) by way of surface reaction oxidizing NO_2 to NO_3^-, field observations needed to support this mechanism have not been unequivocally established. A major difficulty lies in the fact that NO_2 undergoes photochemical

oxidation by OH to form HNO_3 with a characteristic life time < 24 hr. Short of a Lagrangian type of experiment, the contribution of the surface mediated NO_3^- production is difficult to assess. In Figure 17 we plot the percent positive charge due to Ca^{2+} as a function of $[NO_3^-]$. While it is clear that Ca^{2+} played an important role as a neutralizing reagent, accounting for ~50% of the positive charges at $[NO_3^-]$~ 1.5 ppbv, elevated $[NO_3^-]$, i.e., greater than 200 pptv, were nearly exclusively associated with [CO] ≥ 200 ppbv. Under these conditions, HNO_3 formation from photooxidation of NO_2 is typically rapid. Only the C130 data were shown because of the larger Ca^{2+} concentration observed.

Relationship between the ion concentrations and physical measurements. The size and number concentrations of particles were determined using an optical particle counter (OPC) which allowed the surface and volume concentrations of aerosols to be calculated. Having a size cutter implemented, these measurements were segregated into two ranges, the accumulation mode and the coarse mode particles. In Figure 18 we plot the total ion concentrations against the volume concentrations of the accumulation mode particles. Since the PILS cut-off size was estimated to be ~1.3 μm, we expect a good correlation between the total ion mass and the accumulation mode particle volume concentration. Upon a cursory look, one finds that the general agreement between the two quantities is quite reasonable in terms of the magnitudes and a convergence of the data to the origin. However, the spread is considerable, the slope varying between ~0.3 and ~4. Since this slope represents the density of the aerosol particles, those containing high density chemical components should exhibit a steeper slope. This expectation is consistent with the finding that nearly all Ca^{2+} containing samples (cf. density of $CaCO_3$ ≥ 2.7 gm cm^{-3}) lie on the upper range of the data envelope (i.e., $[Ca^{2+}]$ > 0.5 μg m^{-3}). Along this analysis, we noted that the samples with the lowest SO_4^{2-} (i.e., < 4 μg m^{-3}) which contained

almost no Ca^{2+} comprised most of the low slope data points near the bottom of the data envelope. We ignored a group of data points corresponding to a near zero volume but having a total ion concentration as high as 17 μg m^{-3} (along the y-axis) because they may arise from either measurement or calculation errors. This possibility is corroborated with a similar relationship between the volume and absorption at 550 nm.

From the standpoint of density, all of the commonly detected constituents of aerosol including organic compounds (e.g., ammonium formate) have density greater than unity. The less-than-unity-slope data points seen in Figure 18 is due primarily to the incomplete chemical information. We noted from charge imbalance that there is a ~20% (median) of the total ions unidentified. Uncharged components such as PAH's and black carbon can also push the slope up. However, addition of the black carbon mass concentration estimated using a specific absorption coefficient of 10 Mm^2 g^{-1} (Liousse et al., 1993) did not alter the overall picture. The aerosol size cut made on the C130 with which the accumulation mode particles and coarse mode particles were differentiated was variable, ranging between 0.4 and 0.9 μm. We color-coded the data points of Figure 19 to show the effect of this variability: points that show high densities were associated with a smaller size cut compared to those show lower density. Since the PILS sampler is estimated to have a size cut of ~1.3 μm, the data points with a higher size cut should provide a more reliable assessment of the density. The points with smaller size cuts are showing a steeper slope because the aerosol volume concentrations were underestimated compared to the PILS sampling characteristics.

4. Conclusions

Fine aerosol ionic components, NH_4^+, SO_4^{2-}, NO_3^-, K^+, Ca^{2+}, Mg^{2+}, Na^+, and Cl^-, were determined at a 4-min time resolution using a PILS-IC instrument on board the NCAR C130 and

NASA P-3B during the ACE-Asia and TRACE-P experiment, respectively. The maximum total ion concentration observed on the P-3B was 84 μg m^{-3}, significantly higher than that on C130, 27 μg m^{-3}, because of an encounter of highly polluted air mass in the Yellow Sea. The timing and location, however, allowed the C130 to sample air masses that were heavily impacted by dust particles indicated by the elevated Ca^{2+} concentrations (maximum = 6 ppbv). Low levels of Mg^{2+} were also derived from dust at a Mg/Ca ratio of ~ 0.16. Higher levels of Mg were found to have a sea-salt origin showing a Mg/Na ratio of ~0.1. Cl^- and Na^+ were in general correlated, the slope being close to their seawater ratio. Additional sources of Cl^- however were also indicated. SO_4^{2-}, NO_3^-, and K^+ all showed strong correlations with CO, consistent with their origins in combustion. NH_3, which appeared to also be co-emitted from the combustion processes, was in sufficient supply, neutralizing ~70% of the acid aerosols. Charge balance of the 8 detected ions, showed that although the positive and negative charges are tightly correlated, slope ≥ 0.8, the magnitude of the imbalance (positive charge-minus charge, in pptv-eq) was ≥ 20% of the total ion concentration (in pptv). It is expected that these missing charges are associated with organic acids and bases in addition to the hydronium ion. The missing chemical components were mostly likely to be present even in cases where an apparent charge balance were observed. The charge imbalance did not show an altitude dependence and was not dominated by measurement uncertainties. Although the ion concentrations showed a qualitative agreement with a number of aerosol physical properties determined using optical methods, the variability in the size cut with which the accumulation mode particles were characterized (e.g., volume concentration) made direct comparisons less straightforward.

Acknowledgements

This research was supported by NSF and NOAA Office of Climate Change Program for the ACE-Asia Project and by NASA GTE for the TRACE-P Project. The participation of YNL of Brookhaven National Laboratory in the ACE-Asia and TRACE-P was supported by NOAA through an interagency agreement and by NASA through a subcontract with Georgia Institute of Technology, respectively.

References

Andreae, M. O. and P. Merlet. Emission of trace gases and aerosols from biomass burning. Global Biogeochemical Cycles, 15, 955-966, 2001.

Anderson, T. L., S. J. Masonis, D. S. Covert, N. C. Ahlquist, S. G. Howell, A. D. Clarke, and C. S. McNaughton. Variability of aerosol optical properties derived from in-situ aircraft measurements during ACE-Asia. J. Geophys. Res., 2002. This issue. Submitted.

Blake, D. J., D. R. Blake, T.-Y. Chen, J. E. Collins, Jr., G. W. Sachse, B. E. Anderson, and F. S. Rowland. Distribution and seasonality of selected hydrocarbons and halocarbons over the western Pacific basin during PEM-West A and PEM-West B. J. Geophys. Res., 102, 28315-28331, 1997.

Dentner, F. J., G. R. Carmichael, Y. Zhang, J. Lelieveld, and P. Crutzen. Role of mineral aerosol as a reactive surface in the global troposphere. J. Geophys. Res., 101, 22869-22889, 1996.

Fraser, M. P., G. R. Glen, and B. R. T. Simoneit. Gas-phase and particle-phase organic compounds emitted from motor vehicle traffic in a Los Angeles roadway tunnel. Environ. Sci. Technol., 32, 2051-2060, 1998.

Gelencser, A., K. Siszler, J. Jlavay. Toluene-benzene concentration ratio as a tool for characterizing the distance from vehicular emission sources. Environ. Sci. Technol., 31, 2869-2872, 1997.

Howell, S., A. Clarke, R. Weber, S. Masonis, T. Anderson, F. Eisele. Airborne studies of hygroscopic growth in Asian outflow: relations between aerosol size, composition, volatility and related optical properties during ACE-Asia and TRACE-P. J. Geophys. Res., 2002. This issue. Submitted.

Kawamura, K. and F. Sakaguchi. Molecular distributions of water soluble dicarboxylic acids in marine aerosols over the Pacific Ocean including tropics. J. Geophys. Res., 104, 3501-3509, 1999.

Lee, Y.-N., Z. Song, Y. Liu, P. Daum, R. Weber, D. Orsini, N. Laulainen, J. Hubbe, V. Morris. Aerosol chemical characterization on board the doe g1 aircraft using a particle-into-liquid-sampler during the TexAQS 2000 experiment. Extended Abstract published at the 82nd Annual AMS Meeting, Orlando, FL, January 13-17, 2002. Paper no. 10-13.

Liousse, C., H. Cachier, and S. G. Jennings. Optical and thermal measurements of black carbon aerosol content in different environments: variation of the specific attenuation cross-section, sigma (σ). Atmos. Environ., 27A, 1203-1211, 1993.

Ma et al., The characteristics and influence of biomass burning aerosols on fine particle ionic composition measured in Asian outflow during TRACE-P. J. Geophys. Res., this issue, 2002a. Submitted.

Ma et al., Intercomparison of aerosol ionic components measured during TRACE-P and ACE-Asia. J. Geophys. Res., 2002b. Manuscript in preparation.

Marple, V.A., and K. Willeke. Impactor design. Atmos. Environ., 10, 891-896, 1976.

NRC. Research priorities for airborne particulate matter: I. Immediate priorities and a long-range research portfolio. Committee on research priorities for airborne particulate matter, National Research Council, Washington, DC, 1998.

Ooki, A., M. Uematsu, K. Miura, and S. Nakae. Sources of sodium in atmospheric fine particles. Atmos. Environ., 36, 4367-4374, 2002.

Orsini, D. A., Y. Ma, A. Sullivan, B. Sierau, K. Baumann and R. J. Weber. Refinements to the particle-into-liquid sampler (pils) for ground and airborne measurements of water soluble aerosol composition. Atmos. Environ., 2002. Accepted.

Rogge, W. F., M. A. Mazurek, L. M. Hildemann, G. R. Cass, and B. R. T. Simoneit. Quantification of urban organic aerosols at a molecular level: identification, abundance and seasonal variation. Atmos. Environ., 27A, 1309-1330, 1993.

Sachse, G. W., J. E. Collins, Jr., G. F. Hill, L. O. Wade, L. G. Burney, and J. A. Ritter. Airborne tunable diode laser system for high precision concentration and flux measurements of carbon monoxide and methane. Proc. SPIC int. Opt. Eng., 1433, 145-156, 1991.

Seinfeld J. H. and S. N. Pandis. "Atmospheric Chemistry and Physics: From Air Pollution to Climate Change", J. Wiley, New York, 1997.

Sioutas, C., P. Y. Wang, S. T. Ferguson, P. Koutrakis, and J. D. Mulik. Laboratory and field evaluation of an improved glass honeycomb denuder/filter pack sampler. Atmos. Environ., 30, 885-895, 1996.

Thornton, D. C., A. R. Bandy, F. H. Tu, B. W. Blomquist, G. M. Mitchell, W. Nadler, and D. H. Lenschow. Fast airborne sulfur dioxide measurement by atmospheric pressure ionization mass spectrometry (APIMS). J. Geophys. Res., 2002. This issue. Submitted.

Weber, R. J., D. A. Orsini, Y. Duan, Y. -N. Lee, P. J. Klotz, and F. Brechtel. A particle-into-liquid collector for rapid measurement of aerosol bulk chemical composition. Aerosol Sci. Technol. 35, 718-727, 2001.

Weber, R.J., D. Orsini, Y. Duan, Y.-N. Lee, P. Klotz, and F. Brechtel. A particle-into-liquid collector for rapid measurements of aerosol chemical composition. Aerosol Sci. Tech., 35, 718-727, 2001.

Figure Captions.

Figure 1. Schematic diagram of the PILS-IC instrument.

Figure 2. Flight tracks of NCAR C130 and NASA P3-B. The total number of PILS-IC samples are indicated.

Figure 3. Vertical distributions of NH_4^+, NO_3^-, and SO_4^{2-}, and Ca^{2+}, K^+, Na^+, and Cl^- grouped by latitude.

Figure 4. Vertical distribution of total ion mass concentration grouped by latitude. The black lines represent locally weighted average. TRACE-P data points are limited to Lon < 156 deg.

Figure 5. Frequency distributions of aerosol ionic components.

Figure 6. Correlation between aerosol Cl^- and Na^+. The solid lines represent the least squares fits. Data points in the shaded rectangular box were not used in the regression.

Figure 7. Correlation between Mg^{2+} and Ca^{2+}.

Figure 8. Correlation between NH_4^+ and the sum of NO_3^- and SO_4^{2-}. The solid line represents the best fit with data points (in red) showing a significant departure from the main group removed ($r^2 = 0.95$).

Figure 9. Altitude dependence of the ratio of NH_4^+ to the sum of NO_3^- and SO_4^{2-}. The solid curve represents the Lowess average, which approximates the median values. The dotted line is the slope of the best fit in the previous figure. Seventeen points with $[NH_4^+]/([NO_3^-]+2[SO_4^{2-}]$ ratio greater than 5, mostly in the altitude range 5 to 7 km, are not shown.

Figure 10. Ratio of $[NH_4^+]$ to $2[SO_4^{2-}]$ as a function of aerosol sulfate concentration observed during a P-3B volcano plume study. Data are color coded to SO_2 concentration and size coded to altitude (less than 2 km if larger than the smallest point in the graph). The exponential fit of the data is limited to those associated with the Miyakejima volcanic plume using $[SO_2] > 2$ ppbv as a criterion. (SO_2 maximum was 17 ppbv, but clipped at 10 ppbv in the color scale for a better low range resolution.)

Figure 11. Relationship between aerosol SO_4^{2-} and SO_2 in the volcanic plume of Miyakejima. The solid line represents the best fit of the data for $SO_2 > 2$ppbv ($r^2 = 0.80$).

Figure 12. Charge balance of the measured aerosol ionic components during ACE-Asia. Top plot: color-coded to Ca concentration; the solid blue line is the least-square fit of data points. Bottom plot: without Ca^{2+}; the red data points are those identified in Figure 9 as having a large $(NO_3^- + SO_4^{2-})/NH_4^+$ ratio.

Figure 13 . Charge balance of measured ions during TRACE-P. Top plot: Color coded to Ca^{2+} concentration. Bottom plot: color coded to SO_2 concentration; the two lines are the same as those in the top graph.

Figure 14. Charge imbalance of the measured aerosol ionic components as a function of total ion concentration. The solid line represents the best fit of the data and the upper panel shows the deviation of the imbalance from zero normalized to total ion concentration.

Figure 15. Ion imbalance as a function of altitude. Top plots: ACE-Asia. Bottom plot: TRACE-P. Points with a total ion concentration smaller than 500 pptv are shown in solid circles. The solid lines represent Lowess fits to the data.

Figure 16. Correlation between the sum of ions (NO_3^-, SO_4^{2-}, NH_4^+, and K^+) and CO. Top: The group of points showing distinctly low ratios are treated separately; r^2 are 0.82 and

0.54, respectively. The dashed line is the eyeballed top edge of the data envelope. Bottom: The solid line is the best fit of the data without the group with [Ion] < 2 ppbv and [CO] > 300 ppbv. Dashed line is again the eyeballed top of the data envelop and the dotted line is the best fit line of the ACE-Asia data.

Figure 17. Contribution of Ca as a cation as a function of aerosol nitrate concentration.

Figure 18. Relationship between the measured ion mass concentration and the volume of the accumulation mode particles. The data points are color coded to Ca^{2+} concentration truncated at 2 $\mu g\ m^{-3}$ for clarity.

Figure 19. Effect of particle size cut on the relationship between aerosol mass and volume.

Figure 1. Schematic diagram of the PILS-IC instrument.

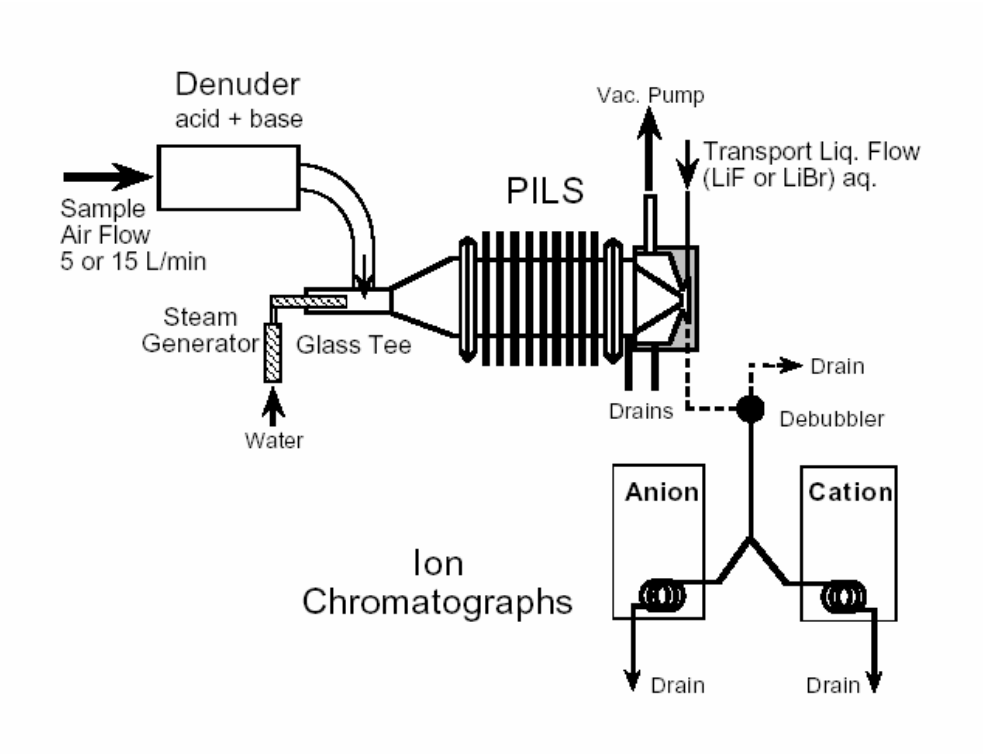

Figure 2. Flight tracks of NCAR C130 and NASA P3-B. The total number of PILS-IC samples are indicated.

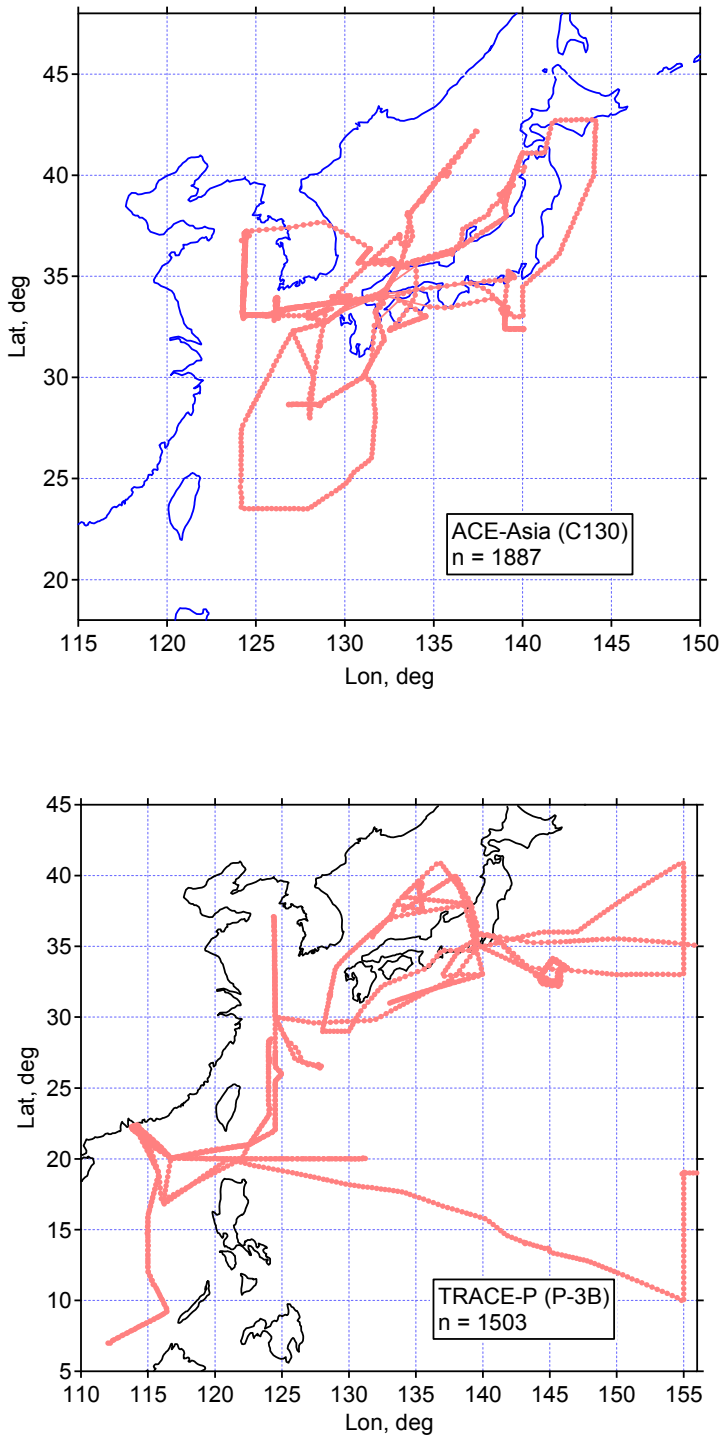

Figure 3. Vertical distributions of NH_4^+, NO_3^-, and SO_4^{2-}, and Ca^{2+}, K^+, Na^+, and Cl^- grouped by latitude.

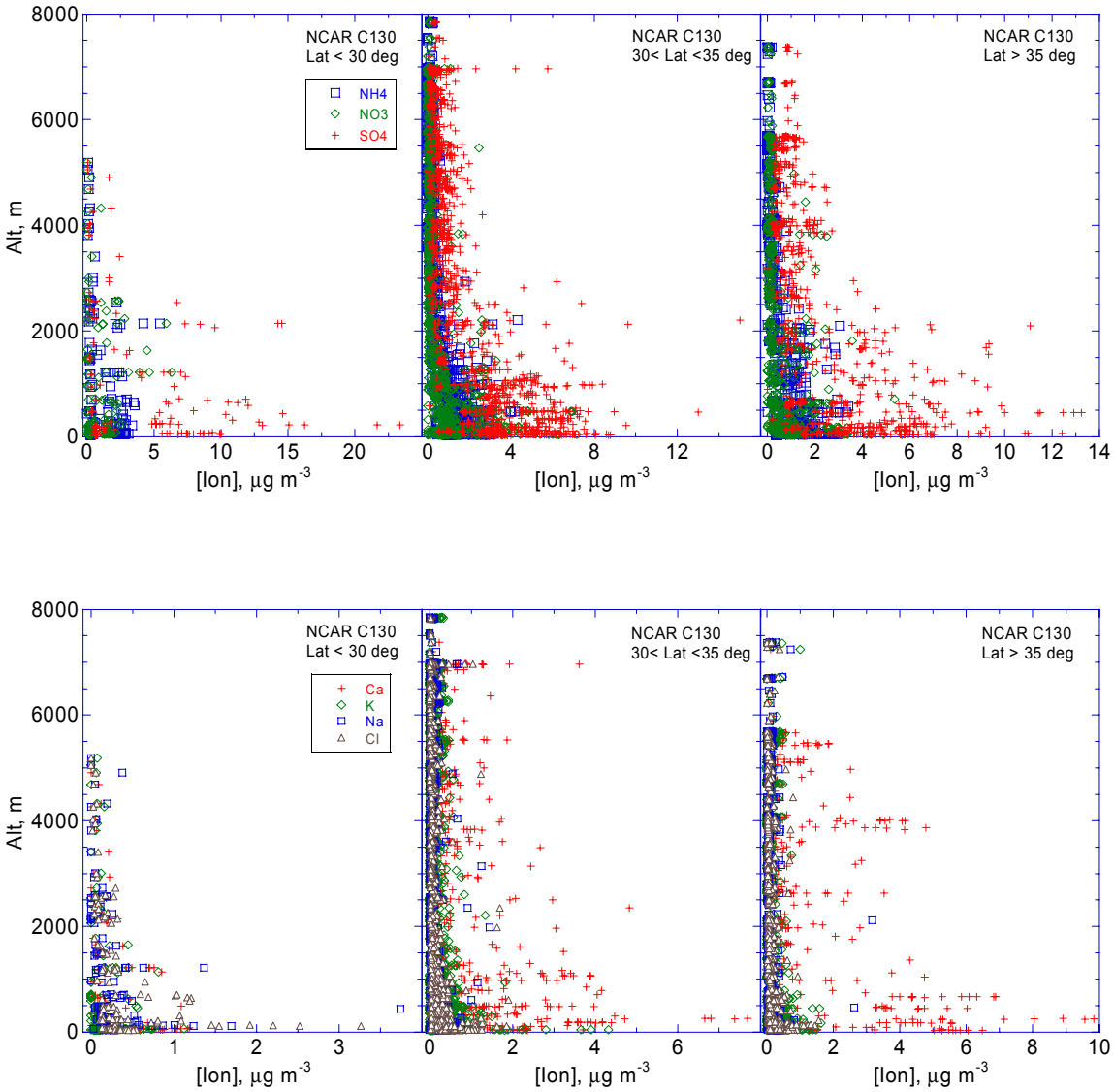

Figure 3. Continued

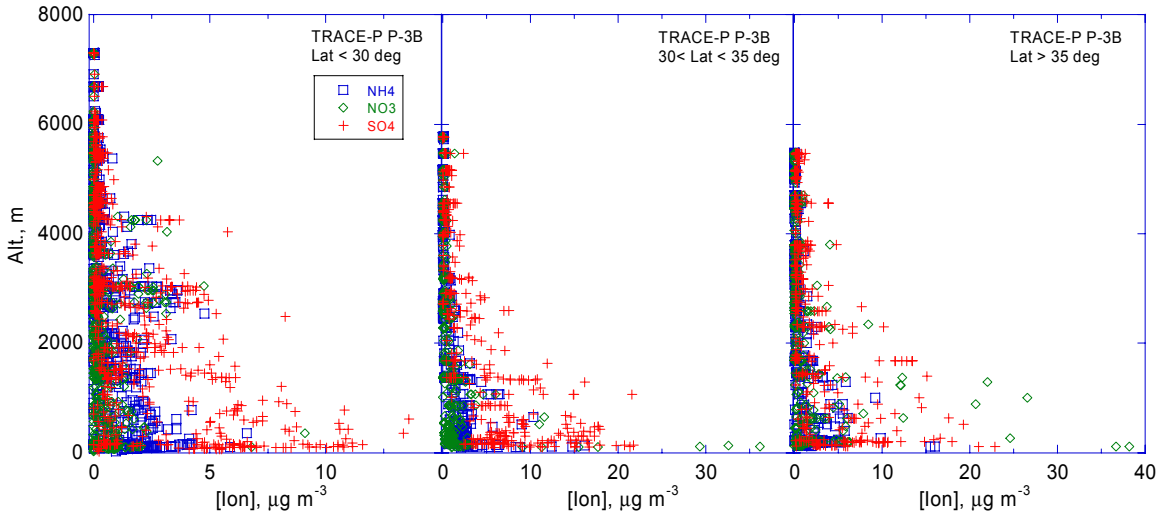

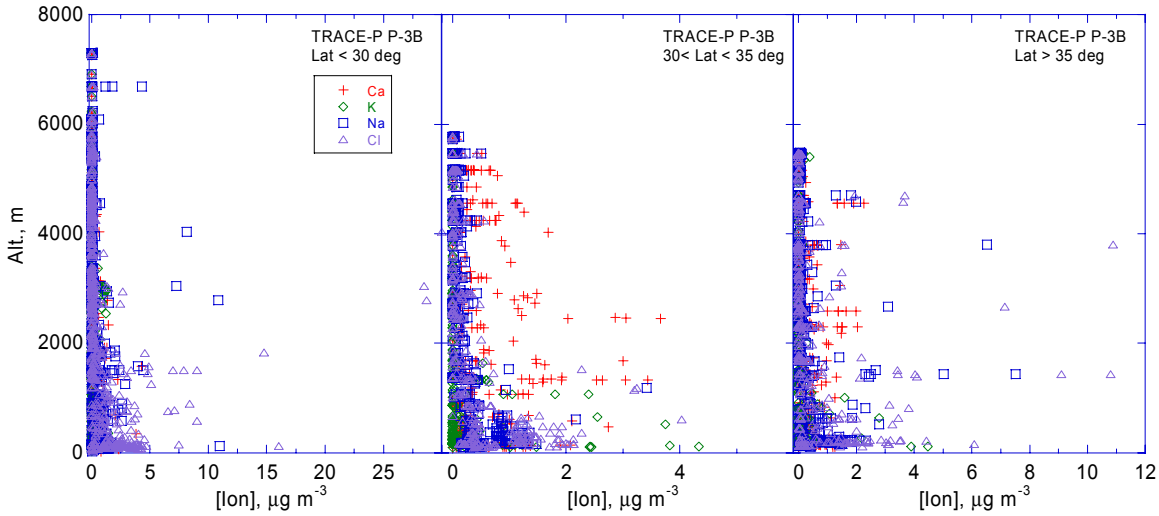

Figure 4. Vertical distribution of total ion mass concentration grouped by latitude. The black lines represent locally weighted average. TRACE-P data points are limited to Lon < 156 deg.

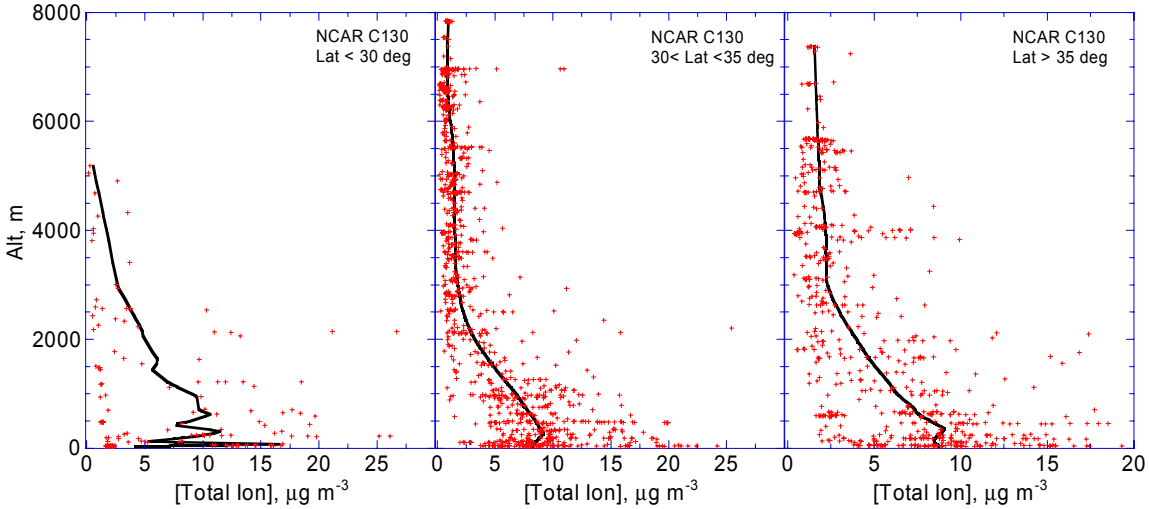

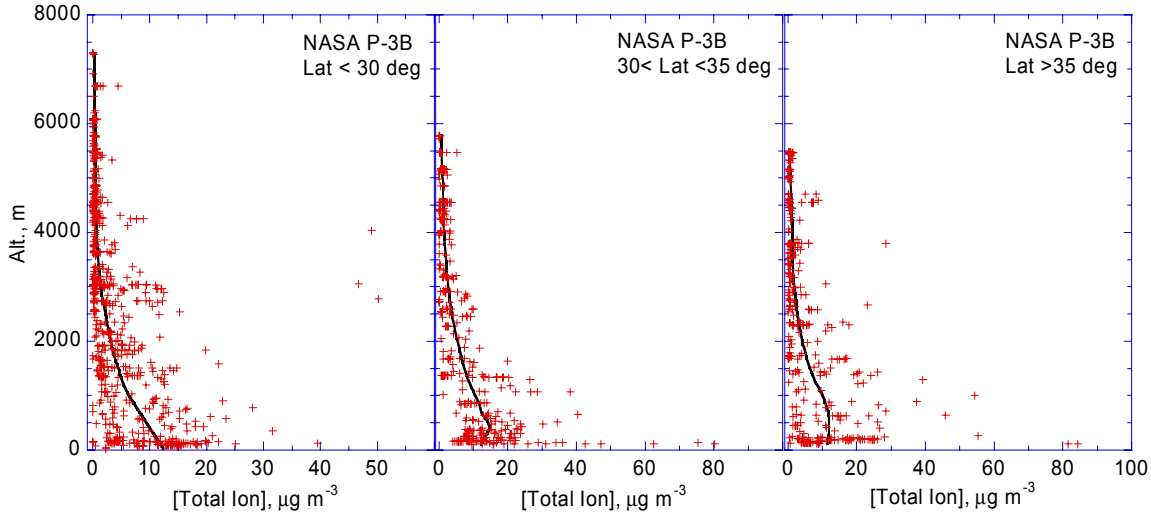

Figure 5. Frequency distributions of aerosol ionic components.

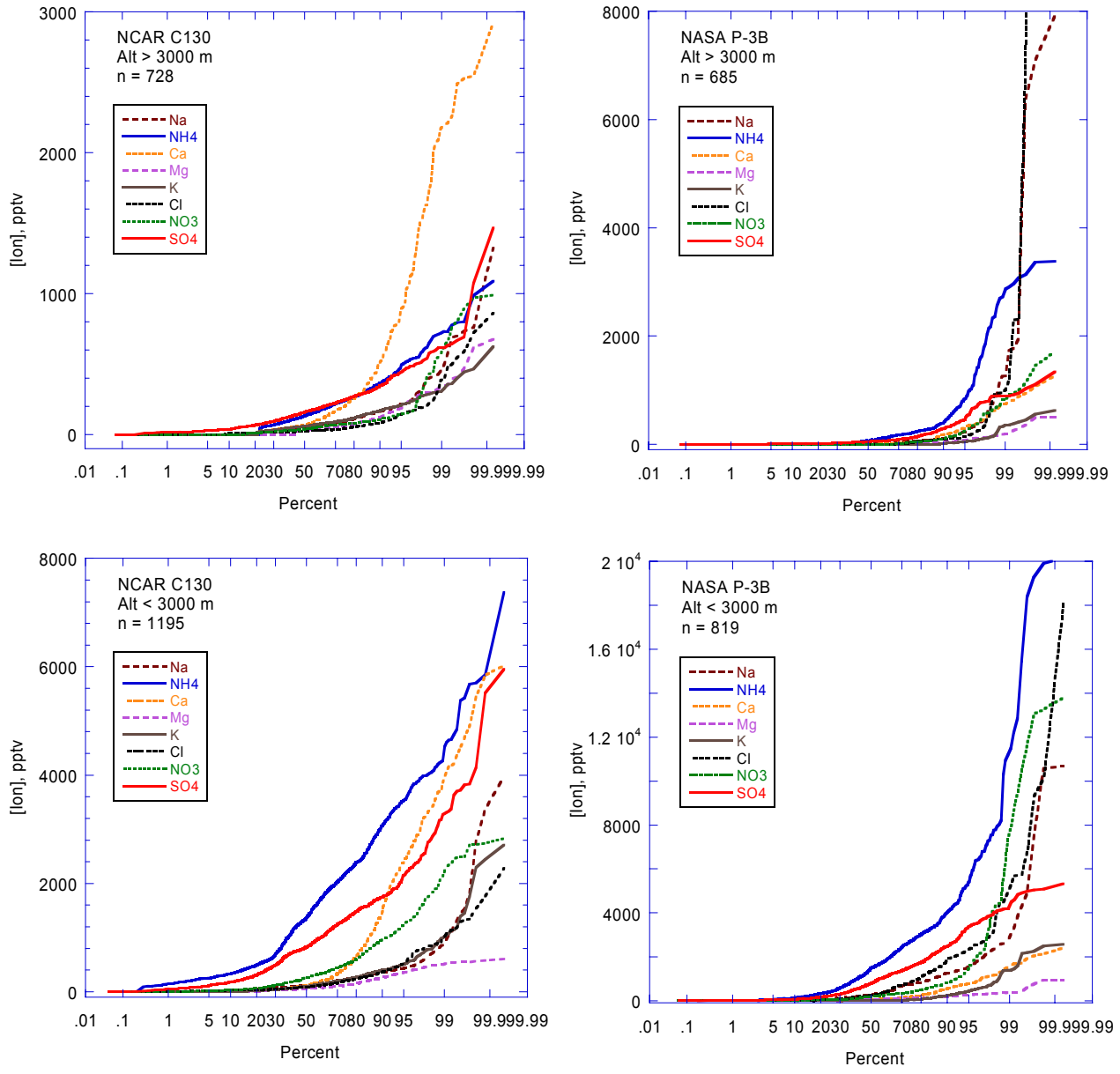

Figure 6. Correlation between aerosol Cl^- and Na^+. The solid lines represent the least squares fits. Data points in the shaded rectangular box were not used in the regression.

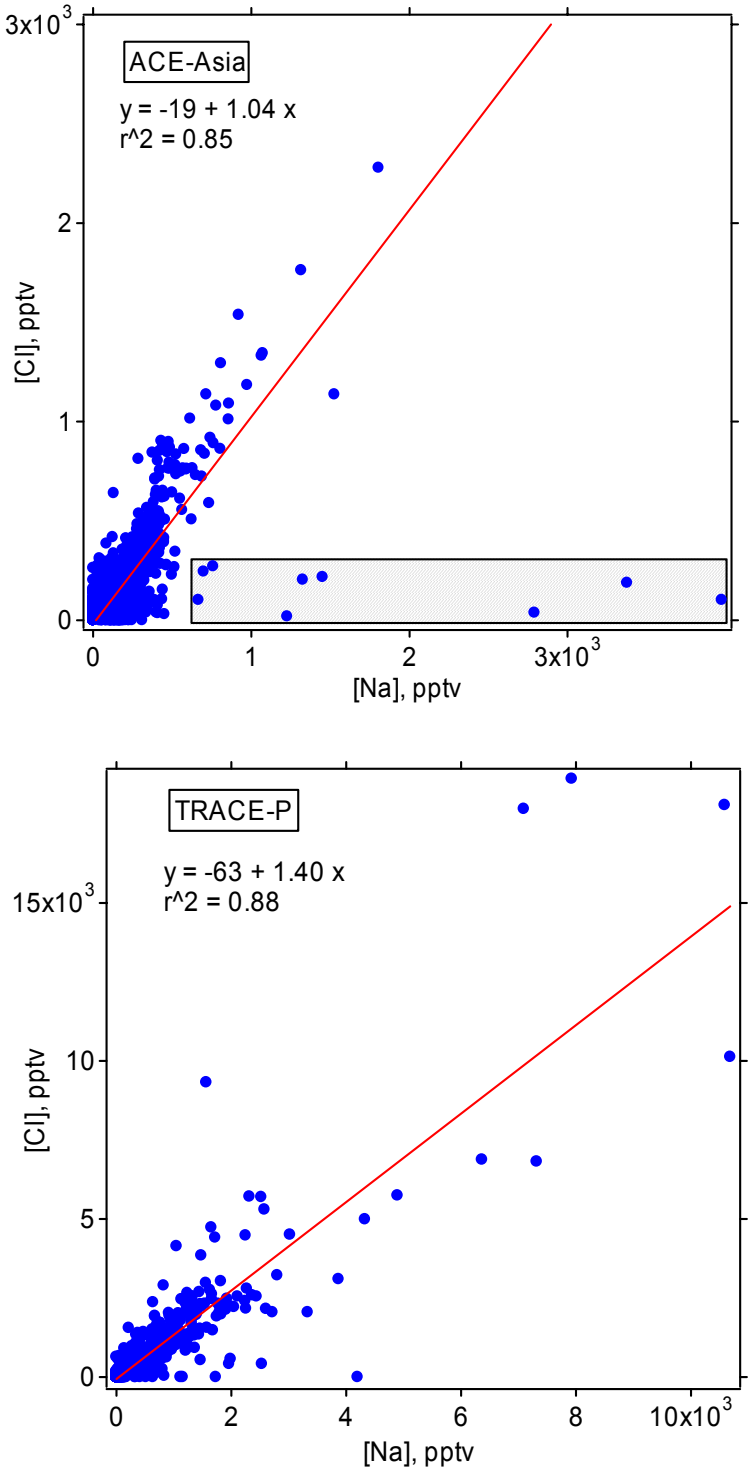

Figure 7. Correlation between Mg^{2+} and Ca^{2+}.

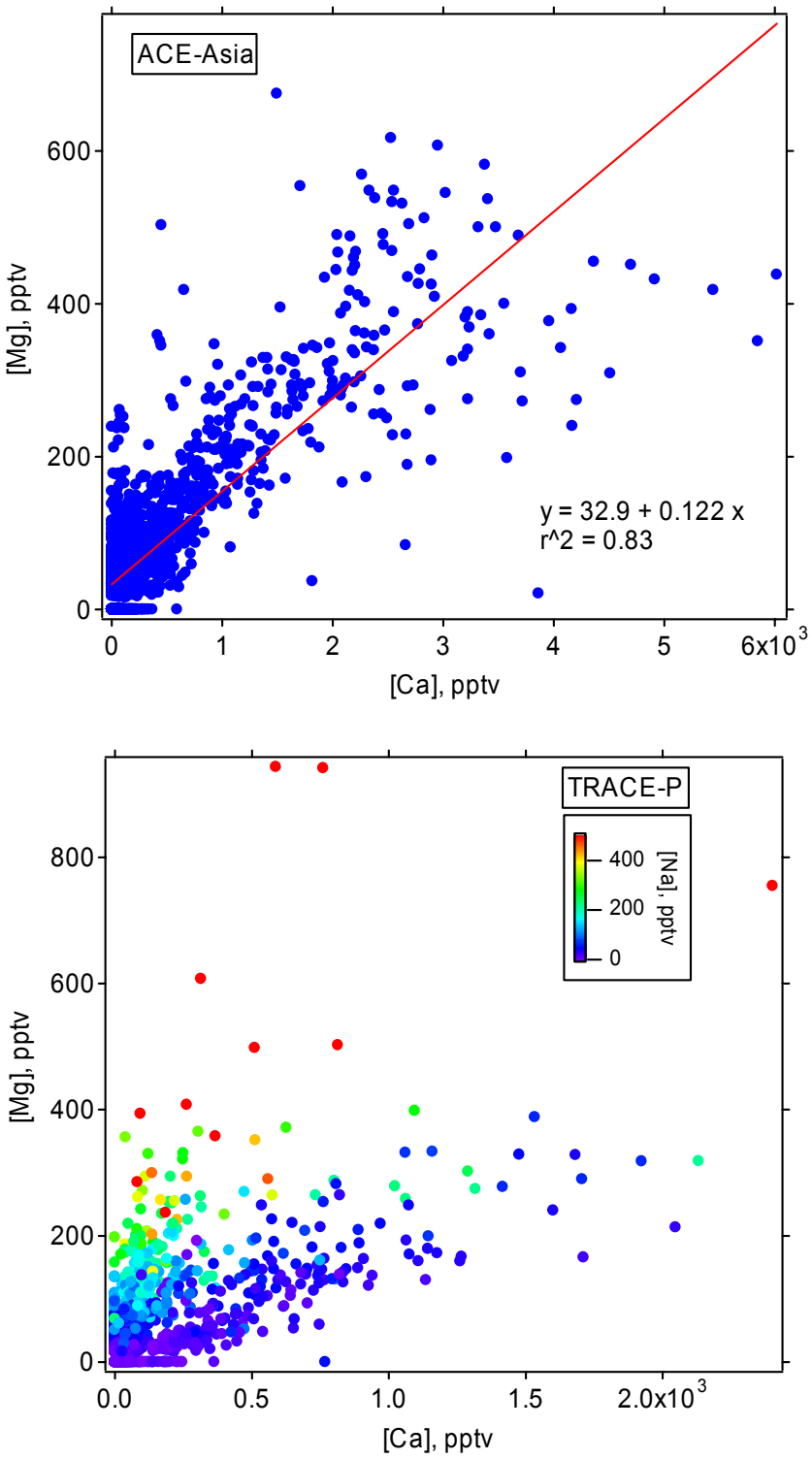

Figure 8. Correlation between NH_4^+ and the sum of NO_3^- and SO_4^{2-}. The solid line represents the best fit with data points (in red) showing a significant departure from the main group removed ($r^2 = 0.95$).

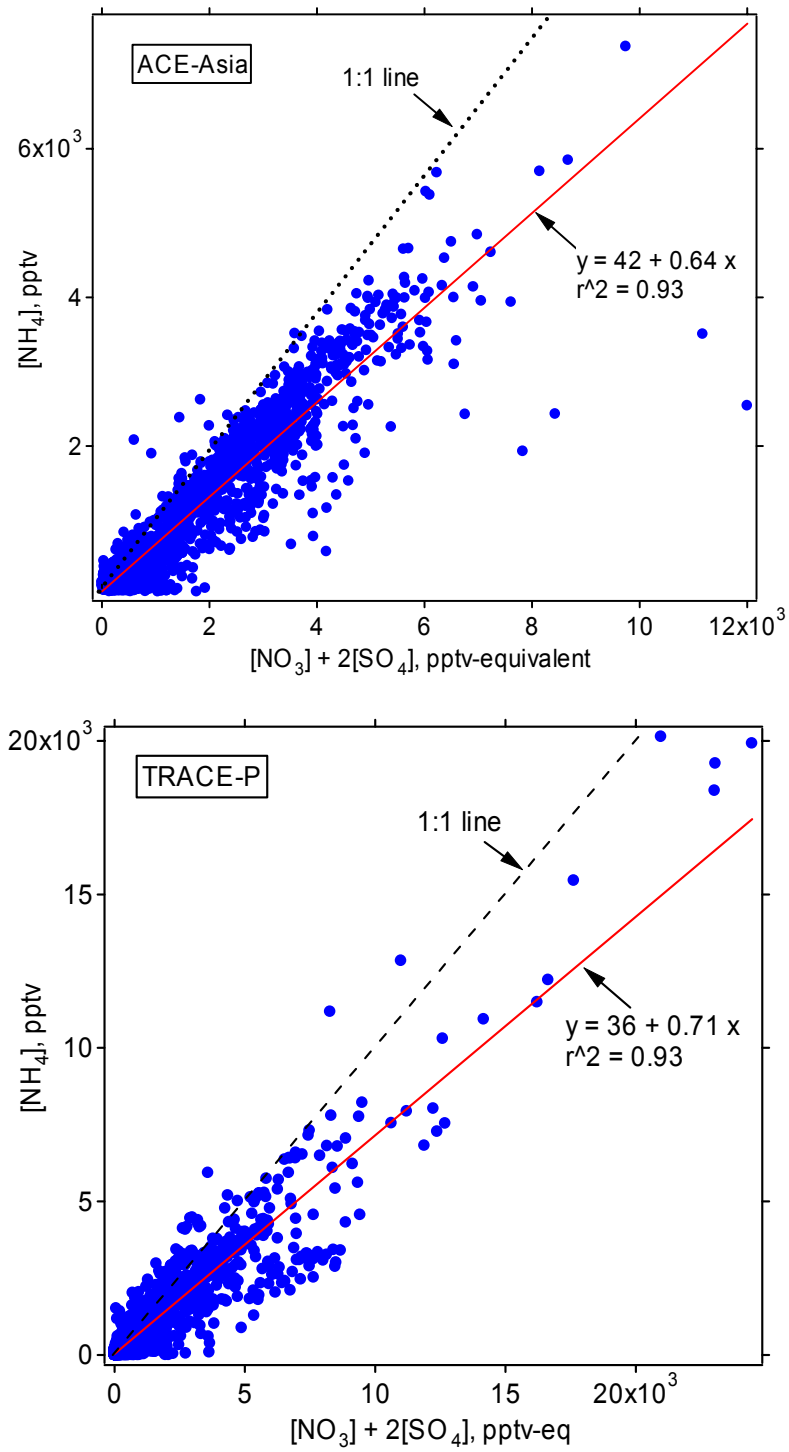

Figure 9. Altitude dependence of the ratio of NH_4^+ to the sum of NO_3^- and SO_4^{2-}. The solid curve represents the Lowess average, which approximates the median values. The dotted line is the slope of the best fit in the previous figure. Seventeen points with $[NH_4^+]/([NO_3^-]+2[SO_4^{2-}]$ ratio greater than 5, mostly in the altitude range 5 to 7 km, are not shown.

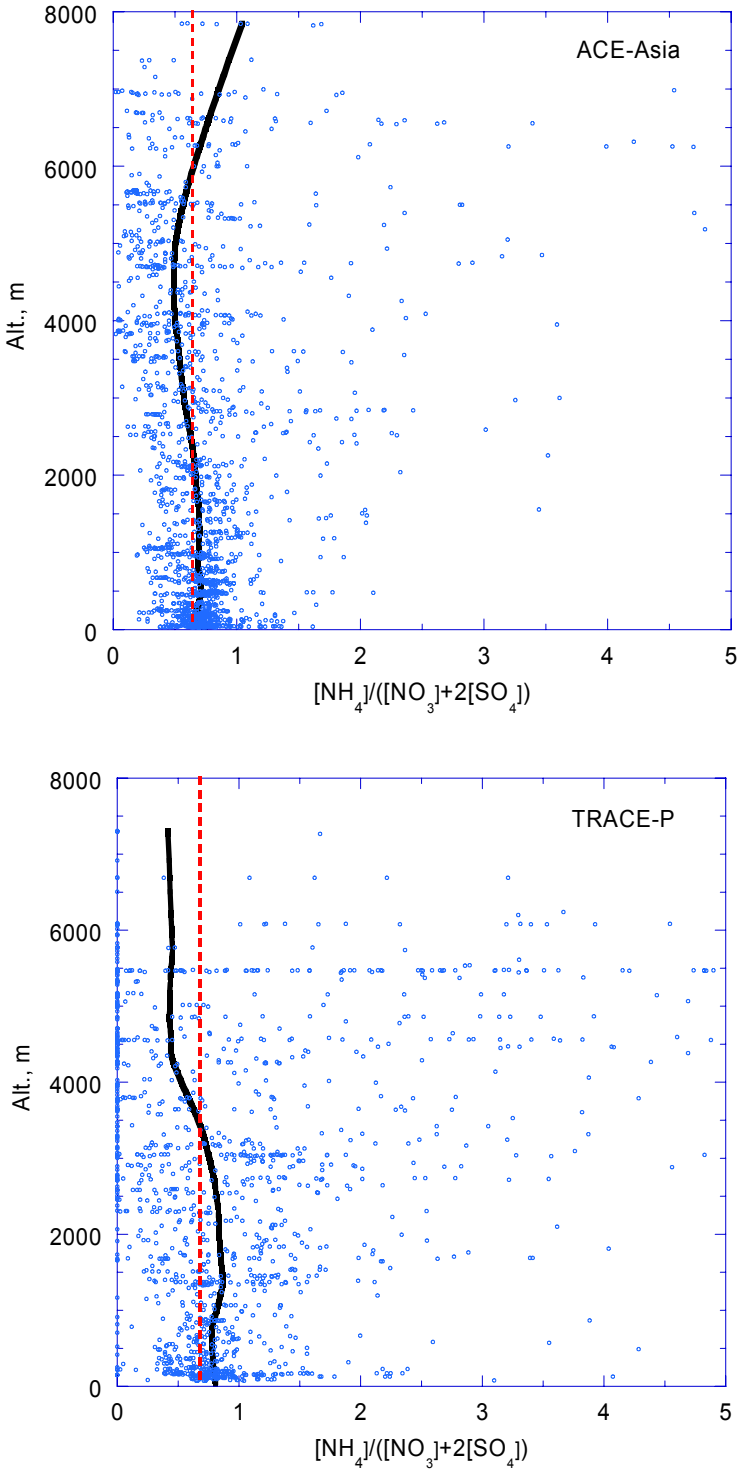

Figure 10. Ratio of $[NH_4^+]$ to $2[SO_4^{2-}]$ as a function of aerosol sulfate concentration observed during a P-3B volcano plume study. Data are color coded to SO_2 concentration and size coded to altitude (less than 2 km if larger than the smallest point in the graph). The exponential fit of the data is limited to those associated with the Miyakejima volcanic plume using $[SO_2] > 2$ ppbv as a criterion. (SO_2 maximum was 17 ppbv, but clipped at 10 ppbv in the color scale for a better low range resolution.)

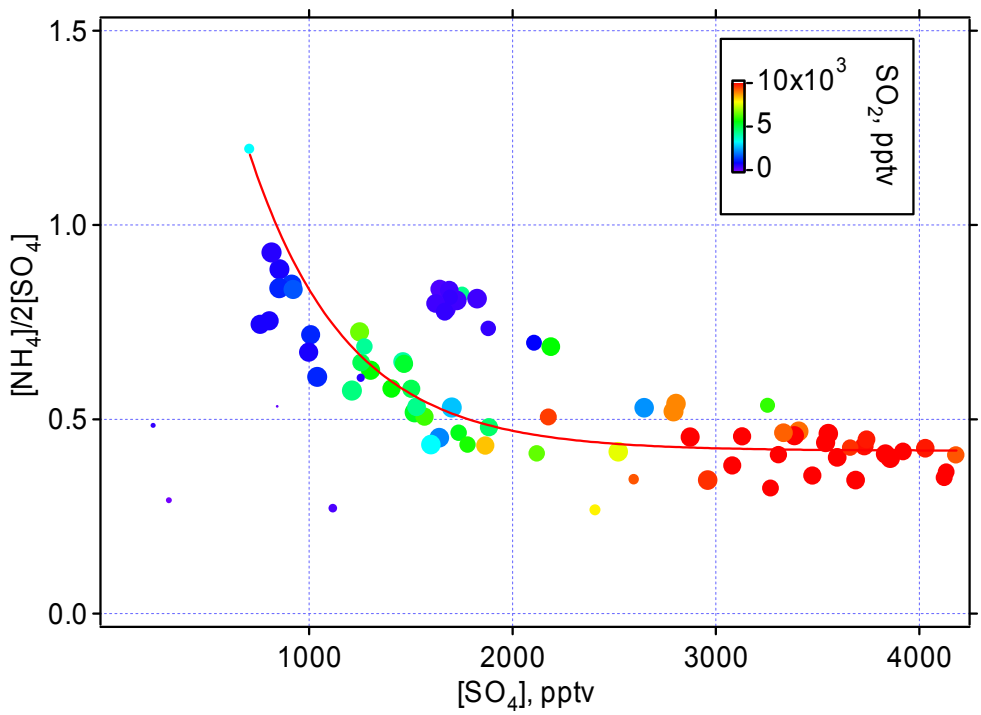

Figure 11. Relationship between aerosol SO_4^{2-} and SO_2 in the volcanic plume of Miyakejima. The solid line represents the best fit of the data for SO_2 > 2ppbv (r^2 = 0.80).

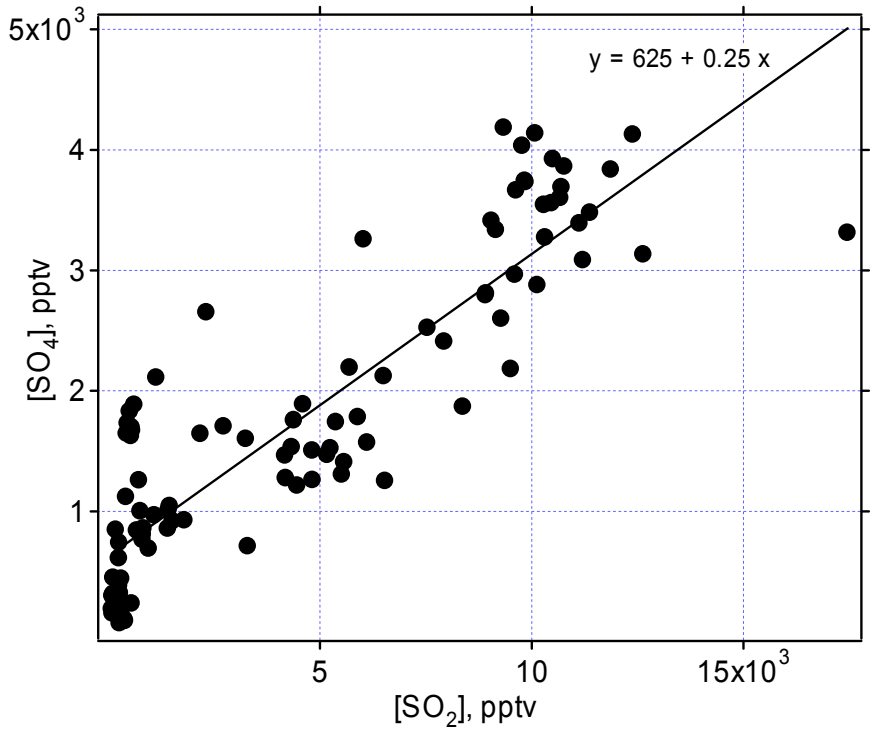

Figure 12. Charge balance of the measured aerosol ionic components during ACE-Asia. Top plot: color-coded to Ca concentration; the solid blue line is the least-square fit of data points. Bottom plot: without Ca^{2+}; the red data points are those identified in Figure 9 as having a large $(NO_3^- + SO_4^{2-})/NH_4^+$ ratio.

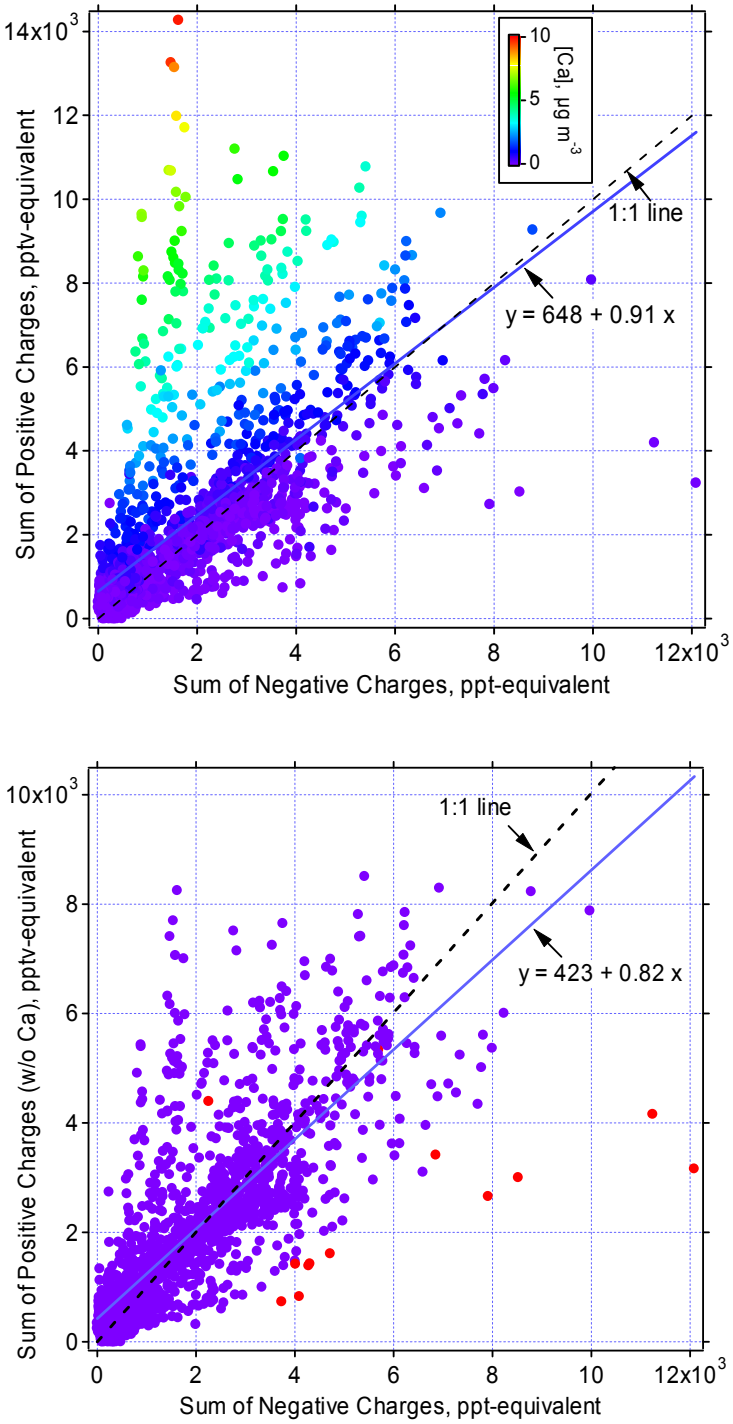

Figure 13 . Charge balance of measured ions during TRACE-P. Top plot: Color coded to Ca^{2+} concentration. Bottom plot: color coded to SO_2 concentration; the two lines are the same as those in the top graph.

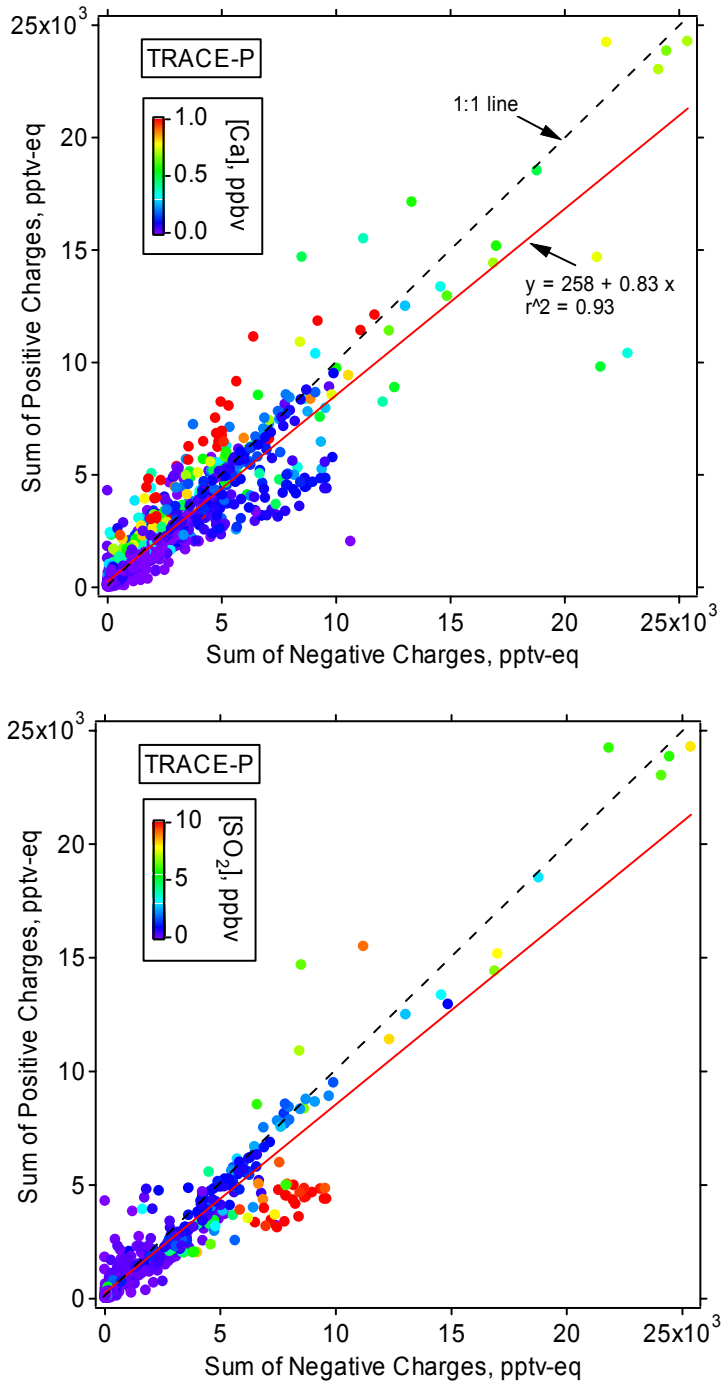

Figure 14. Charge imbalance of the measured aerosol ionic components as a function of total ion concentration. The solid line represents the best fit of the data and the upper panel shows the deviation of the imbalance from zero normalized to total ion concentration.

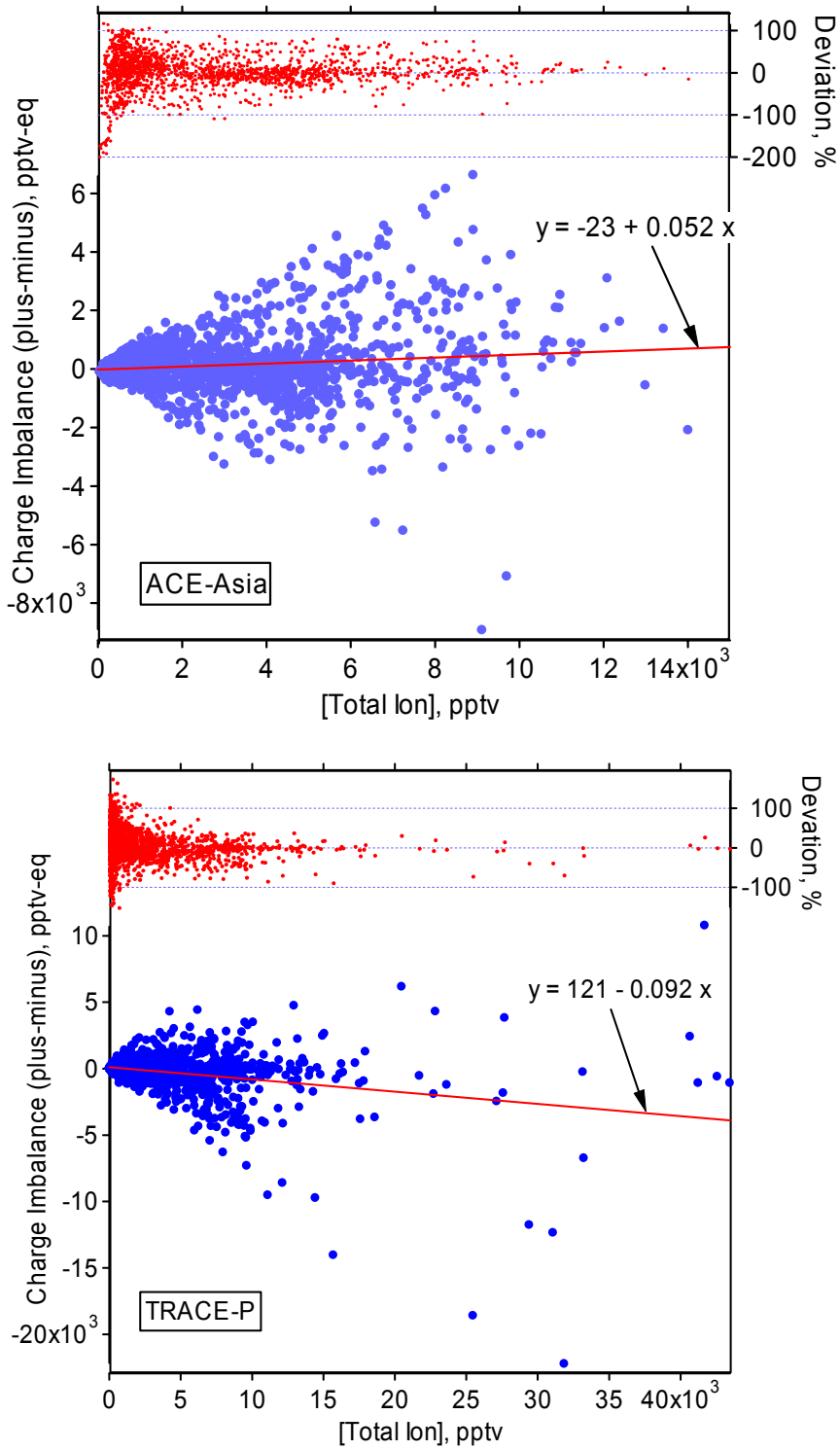

Figure 15. Ion imbalance as a function of altitude. Top plots: ACE-Asia. Bottom plot: TRACE-P. Points with a total ion concentration smaller than 500 pptv are shown in solid circles. The solid lines represent Lowess fits to the data.

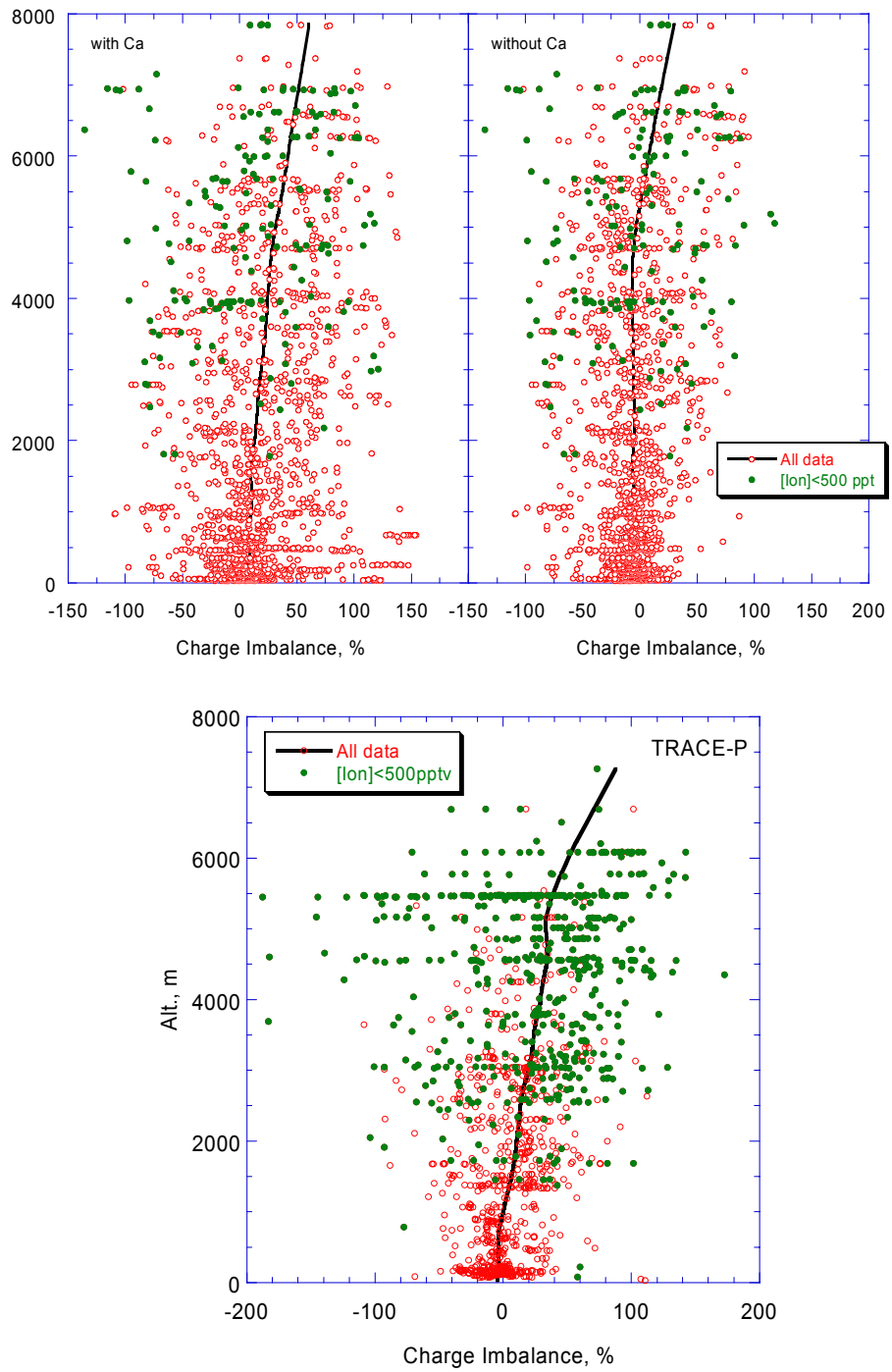

Figure 16. Correlation between the sum of ions (NO_3^-, SO_4^{2-}, NH_4^+, and K^+) and CO. Top: The group of points showing distinctly low ratios are treated separately; r^2 are 0.82 and 0.54, respectively. The dashed line is the eyeballed top edge of the data envelope. Bottom: The solid line is the best fit of the data without the group with [Ion] < 2 ppbv and [CO] > 300 ppbv. Dashed line is again the eyeballed top of the data envelop and the dotted line is the best fit line of the ACE-Asia data.

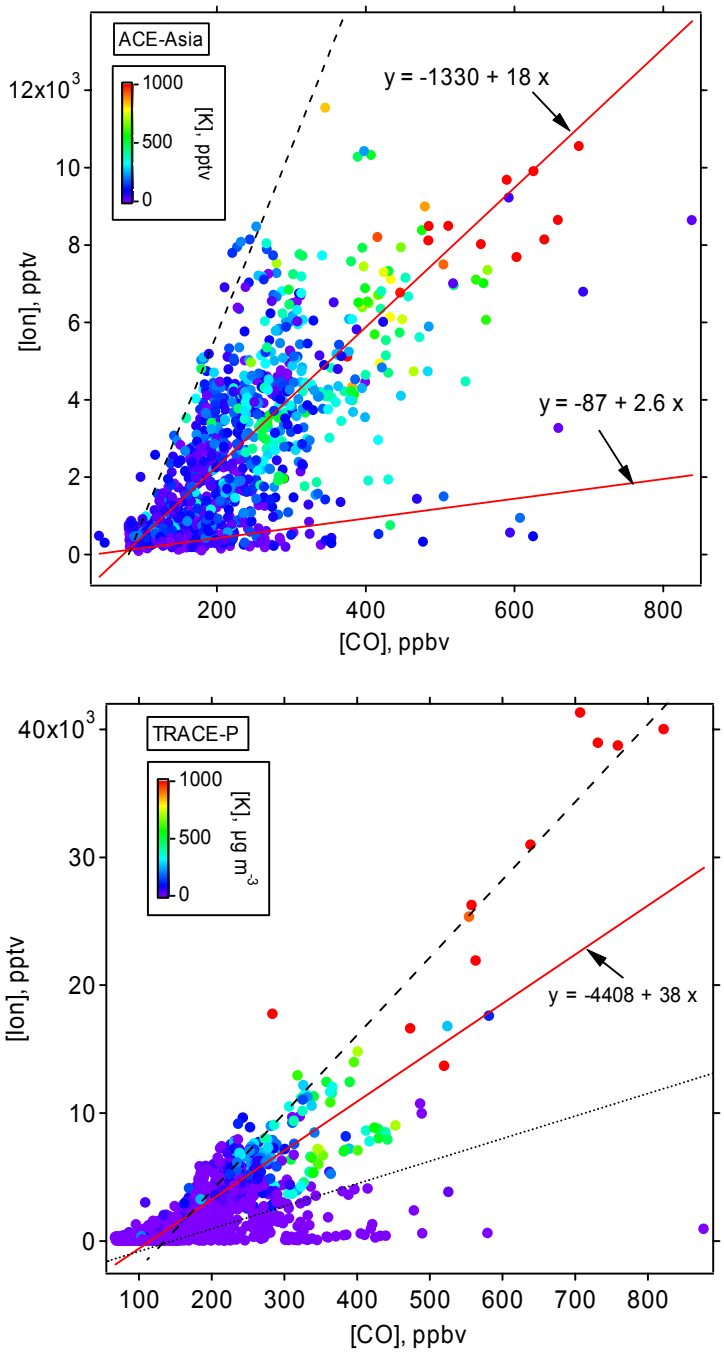

Figure 17. Contribution of Ca as a cation as a function of aerosol nitrate concentration.

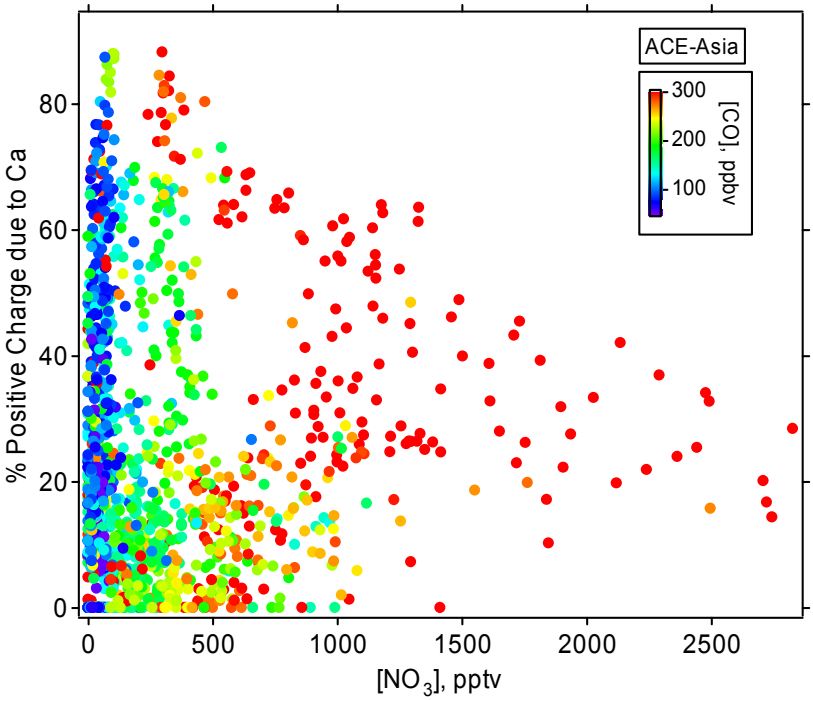

Figure 18. Relationship between the measured ion mass concentration and the volume of the accumulation mode particles. The data points are color coded to Ca^{2+} concentration truncated at 2 μg m^{-3} for clarity.

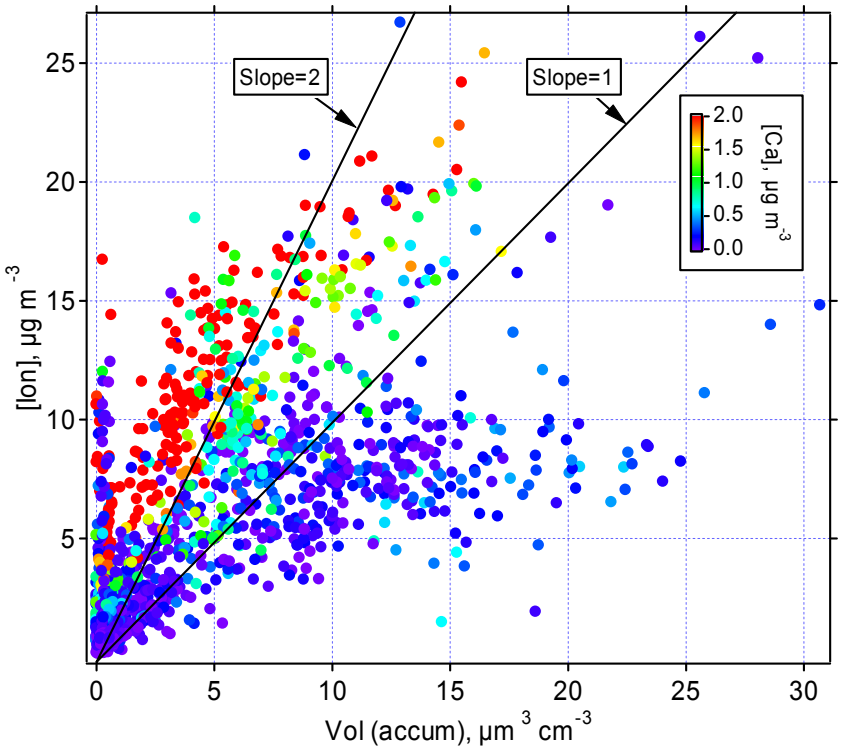
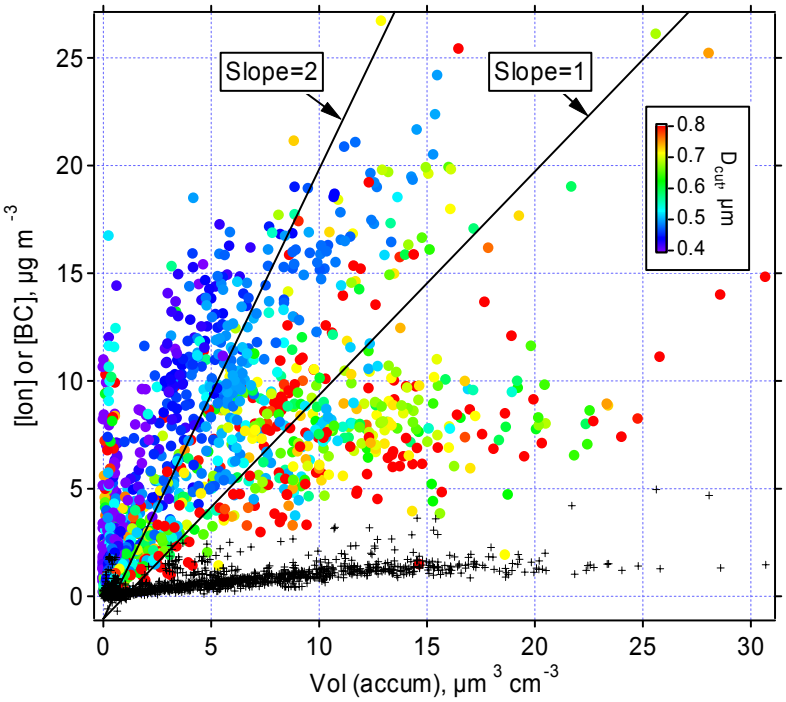
Figure 19. Effect of particle size cut on the relationship between aerosol mass and volume.